Eksploatacja i Niezawodnosc - Maintenance and Reliability
Volume 29 (2027), Issue 1
https://ein.org.pl
The Polish Maintenance Society

Measurement and analysis of dynamic performance of shearer cutting part transmission system under different working conditions using simulation method

Kuidong Gao[1], Zhiteng Liu[1], Guanzhan Dong[1], Xiaodi Zhang[1,*], Liqing Sun[1], Shengru Zhang[1], Tianyu Liu[1]

[1] College of Mechanical and Electronic Engineering, Shandong University of Science and Technology, Qingdao 266590, China
* Corresponding Author: zhangxiaodi@sdust.edu.cn

Received: 8 May 2026
Revised: 15 May 2026
Accepted: 21 May 2026
Online: 8 July 2026

This is an open access article under the CC BY 4.0 license

Abstract

As key coal mining equipment, the shearer is crucial for improving adaptability to complex conditions, extending service life, and reducing failure rates—key to enhancing coal production economic benefits. Using the transmission system model, dynamic bearing contact forces, vibration acceleration at virtual measurement points, and vibration levels in gangue/pure coal conditions are analyzed. The reliability and accuracy of the finite element analysis for the cutting unit's vibration characteristics were validated via bench test comparison. The vibration-data-equipped housing is input into acoustic boundary element simulation; combined with the built model, noise variations at different sound field response points with gear face width and bottom clearance coefficient are derived. Results show high-order modal analysis confirms no system resonance risk. When the motor gear face width is 74 mm, planetary gear train face width 140 mm, and bottom clearance coefficient 0.4, the gears exhibit excellent load-bearing capacity, stability, and low vibration/noise.

Keywords: *shearer, cutting unit transmission system, dynamic analysis, modal analysis, vibration noise measurement*

Article citation:
Gao K, Liu Z, Dong G, Zhang X, Sun L, Zhang S, Liu T, Measurement and analysis of dynamic performance of shearer cutting part transmission system under different working conditions using simulation method. Eksploatacja i Niezawodnosc – Maintenance and Reliability 2027: 29(1) http://doi.org/10.17531/ein/222328

Highlights

- Test-simulation comparison verifies shearer cutting unit vibration simulation reliability.
- Modal analysis shows first 40 natural frequencies avoid resonance.
- Optimize gear parameters to reduce vibration and noise.
- LMS Virtual.Lab acoustic boundary element simulation analyzes noise distribution.

1. Introduction

With the development of high-reliability, high-efficiency, and low-energy-consumption fully mechanized mining equipment, shearers have become the core equipment for coal seam cutting. Optimizing their performance under complex conditions, improving measurement accuracy, and reducing failure rates are critical to enhancing coal production economics [1]. Single-motor driven shearer cutting units have a simple transmission structure and were widely used in early medium-thick coal seam mining, where a single motor transmits power to the drum via gear trains [2]. However, in thin coal seams with limited cutting height, increasing cutting power often requires a longer transmission chain, leading to larger structural dimensions and reduced adaptability to confined spaces. Additionally, in complex coal seams, a single motor bears most of the machine's power, concentrating instantaneous impact loads and causing high failure rates in high-speed gears and reducers, making it difficult to meet efficient and reliable mining needs [3]. In contrast, in thin coal seam fully mechanized faces, a dual-motor series-driven shearer can increase cutting power without lengthening the transmission chain, effectively adapting to limited cutting height. The dual-motor configuration splits the total power, reducing load concentration on individual motors and transmission components, thereby ensuring more stable operation and improving measurement accuracy under strong instantaneous impacts and large alternating load fluctuations [4].

Consequently, this system is increasingly used in thin coal seam mining. However, practical applications still face challenges: complex coal seam conditions and large cutting load impacts lead to high failure rates in high-speed spur gears and planetary reducers. Meanwhile, vibration and noise not only worsen the working environment but also reduce equipment bearing capacity. High maintenance costs and measurement difficulties severely restrict technological development [5]. Against this background, this paper investigates the dynamic characteristics, bearing performance, and vibration and noise behavior of the dual-motor cutting unit's transmission system. It measures transient impacts, tooth surface meshing, vibration, noise, and other related characteristics under multiple influencing factors, aiming to provide a reference for improving the working condition adaptability and bearing capacity of thin coal seam shearers.

In recent years, the study of gear dynamics is no longer limited to a single analytical method or a full finite element method. The research objects are also from spur gears to new gears, such as herringbone gears, spherical gears and logarithmic gears. And for the study of gear vibration and noise, experimental testing and simulation are widely used in engineering. Jin et al. [6] numerically studied the natural vibration of a planetary gear system using a multi-DOF time-varying dynamic model, calculating natural frequencies and modes. They verified the effects of carrier speed and support stiffness on natural characteristics, but only for low-order modes. Simon et al. [7] proposed holographic image replication for multi-point real-time vibration measurement with a resolution of 100 nm in amplitude and 1000 Hz in frequency. However, its reliance on optical equipment makes it difficult to adapt to harsh underground environments with dust and humidity, limiting engineering practicality. Marcos et al. [8] obtained vibration acceleration and acoustic spectrum data via multi-body dynamics simulation and validated a combined simulation–neural network approach. However, measuring points were only placed at the end of a single gear shaft, failing to capture coupling vibrations of the high-speed stage and planetary gear train under strong impact. Zhu et al. [9] established a bending-torsional coupled vibration model of a dual-input single-output cylindrical gear system under synchronous and asynchronous meshing, considering multiple nonlinear factors, and analyzed the influence of meshing frequency on vibration. Huang et al. [10] studied the dynamic behavior of hypoid gears under periodic tidal energy harvesting, finding that second-order primary resonance intensity is high under reverse input conditions, which is significant for power efficiency and acoustic radiation. Guan et al. [11] developed a finite element model of gears with manufacturing errors, but the vibration response calculation did not incorporate dynamic load measurement data under actual operating conditions; model validation relied on ideal load assumptions. Song et al. [12] used operating deflection shape analysis and experimental modal analysis to trace the transmission path. By controlling hypoid gear tooth profiles, they reduced transmission error and shafting excitation forces, significantly lowering howling noise. Zhou et al. [13] established linear and nonlinear vibration-impact models of a transmission system considering time-varying meshing stiffness and other factors to obtain dynamic loads, then derived vibration and noise radiation characteristics of the reducer using FEM/BEM. D. Schweigert et al. [14] developed, manufactured, and tested a high-speed planetary gearbox, comparing numerical frequency response analysis with bench tests, and verified the feasibility of the excitation calculation method. Hamza et al. [15] used the potential energy method to establish a gear friction dynamics model for gear whine problems, capturing harmonic and superharmonic resonances with accurate amplitude and frequency. Damian et al. [16] developed a lubrication-aware FE dynamic model of an EV steering assembly, showing that contact parameters from static/quasi-static/low-speed analyses are unsuitable for NVH impact analysis—nonlinear contact stiffness with damping under lubrication yields better results. Hong et al. [17] analyzed the influence of gear web holes on noise using LMS Virtual.Lab, but the sound field simulation only employed a planar field point grid, which could not characterize 360° omnidirectional noise radiation of a shearer, and noise assessment in key areas was missing. Huang et al. [18] established a rigid-flexible coupled dynamic model of a construction elevator transmission system. Using Romax, they simulated acoustic power and obtained a maximum noise value of 78.8 dB. Tanaka et al. [19] calculated reducer radiation noise using the boundary element method with a semi-free field simplification. However, in an actual fully mechanized mining face, the coal wall's sound

reflection coefficient of 0.8–0.9 results in measured noise values being 8-12 dB(A) lower than actual field values.

Current gearbox modal analysis mostly focuses on low-order modes, neglecting fundamental/harmonic frequency effects under time-varying excitation—high-frequency modes may be excited to cause resonance. Thus, system resonance research should fully consider support shaft rotational frequency, gear pair meshing frequency, and high-order harmonics. Existing acoustic boundary element simulations usually adopt semi-free field-based sound field points, which save computing resources but ignore noise radiation omnidirectionality. Therefore, studies on the shearer cutting unit's gear transmission system should incorporate actual shearer noise radiation characteristics and use spherical field point grids. To address these gaps, this paper uses the gear-shaft system NVH module in Romax for modal analysis of the cutting unit's transmission system, identifying potential resonant modes by focusing on modes near the excitation's fundamental and harmonic frequencies. It then obtains system vibration data via virtual measuring points to evaluate vibration levels under different working conditions. Finally, the housing with vibration data is imported into LMS Virtual.Lab as boundary conditions for acoustic boundary element simulation, realizing noise characteristic analysis.

2. Construction of dynamic model of shearer cutting unit transmission system under different working conditions

To study the dynamic performance of the shearer cutting part transmission system and verify the effectiveness of the simulation method, this section first built a comprehensive test bench for the shearer gear transmission system to carry out dynamic performance tests, then established a finite element model in Romax and verified its reliability by comparing test and simulation results, and finally constructed a dynamic model and a near-field acoustic model of the MG2×250/1200-WD shearer cutting part transmission system, and obtained the load characteristics under different working conditions by LS-DYNA.

2.1. Feasibility verification of dynamic simulation method for shearer cutting unit by Romax

2.1.1. Experimental study on dynamics of shearer-like cutting unit transmission system

The comprehensive test device of shearer cutting unit transmission system is composed of gear transmission system, load loading system, sensing acquisition system, platform lifting system and control system, as shown in Figure 1. The transmission distribution at all levels is shown in Table 1.

The comprehensive test bench for the shearer's gear transmission system is highly consistent with the working principle of the cutting unit. It is scaled down proportionally based on the similarity theory, which not only improves space utilization but also accurately reflects the dynamic characteristics of the cutting unit's transmission system. Equipped with a mine-used flameproof three-phase asynchronous motor, it enables equipment start-stop and speed control. A magnetic powder brake is adopted to apply a torque of 0-2000 N·m for simulating actual loads. Relying on an Ethernet sensor network, it realizes multi-interface compatible data collection for sensors measuring acceleration, temperature, etc. Three servo electric cylinders are used for cross-coordinated control to simulate the shearer cutting coal seams of different heights. Additionally, it is equipped with a control system to achieve centralized control of multiple systems, as well as data storage and display. Scholars at home and abroad have conducted extensive research on the dynamic characteristics of shearer gear transmission systems, and have carried out single-aspect analysis and verification by building test devices. However, these studies fail to comprehensively and accurately reflect the actual operating conditions of the shearer's gear transmission system [20]. The construction of this test bench can accurately reflect the operating status of the shearer's gear transmission system and conduct comprehensive detection of faults in the gear transmission system. By simulating the lifting angle of the rocker arm through electric cylinders, with the motor power being above 20 KW and the speed regulation range of 0-1500 rpm, it can collect more than 8 types of transmission characteristics of the shearer's gear system, including vibration, temperature, inclination angle, rotational speed, as well as oil viscosity, density, dielectric constant, and abrasive particles.

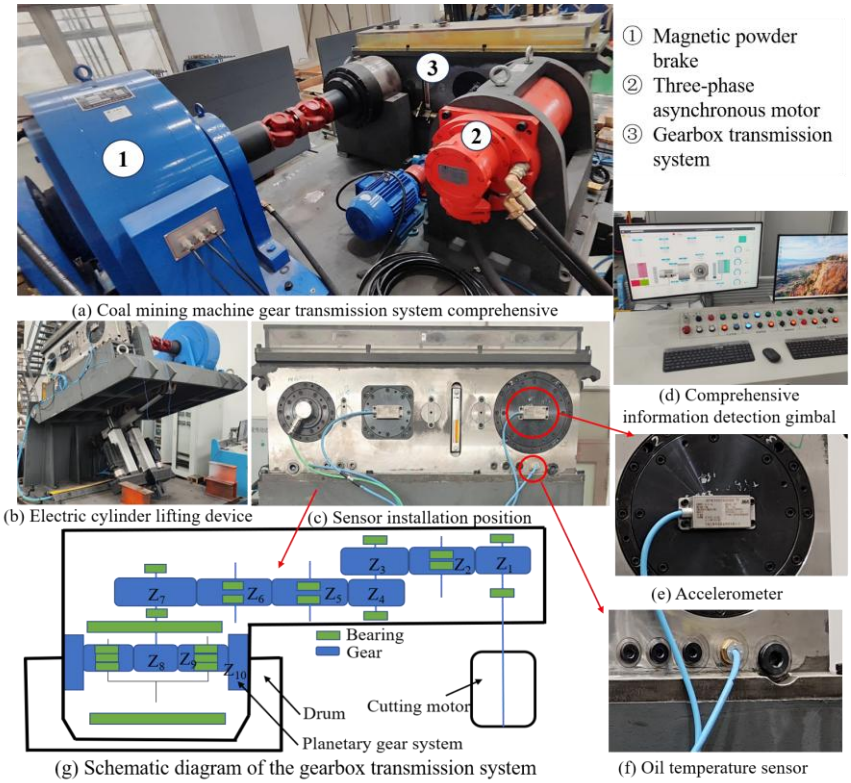

Figure 1. Shearer gear drive system comprehensive test equipment.

Table 1. Transmission distribution table at all levels of the test equipment.

Gear number	Z_1	Z_2	Z_3	Z_4	Z_5	Z_6	Z_7	Z_8	Z_9	Z_{10}
Quantity	1	1	1	1	1	1	1	1	4	1
Tooth number	28	41	39	27	37	37	40	15	24	65
Rotational speed	739	506.732	532.663		388.700		359.585		67.422	0
Rotational frequency	12.37	8.45	8.78		6.48		6		1.12	
Transmission ratio		1.393			1.481				5.333	
Module		4			5				4	
Mesh frequency		346.27			239.70				89.90	

In this test, the input speed is set to 739 r/min, and the rated load torque is 1364 N·m. By controlling the operation interface of the test bench, the vibration signal during the experiment is collected by the sensing system of the test bench. The three acceleration sensors are located above the one-axis, three-axis end cover and the ring gear shaft shell of the planetary gear train. As shown in Figure 2, the A196, A197 and A201 simulation channels simulate the motor shaft end cover, the three-axis end cover and the shell directly above the ring gear in the planetary gear train. The x, y and z directions at the one-axis and three-axis end cover indicate the horizontal, gravity and axial directions of the test bench, while the x, y and z above the planet carrier shell indicate the horizontal, axial and gravity directions of the test bench. In order to avoid the aliasing effect caused by the mapping of high frequency signal to low frequency signal, the sampling frequency is set to 10000 Hz, and three analog channels are set to collect the acceleration vector data in x, y and z directions respectively [21]. After the power system is stable, the 2s data is intercepted, and the vibration acceleration curve in the time domain under different working conditions is obtained as shown in Figure 3.

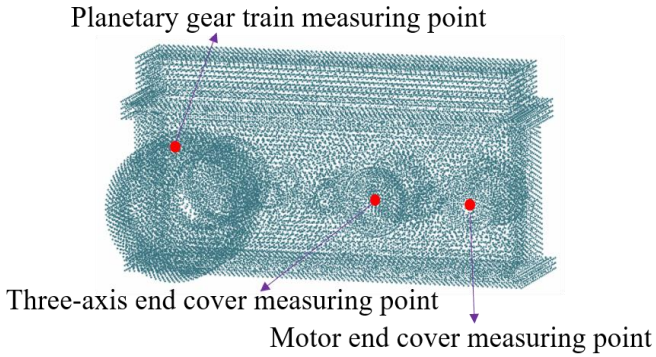

Figure 2. Test bench shell measuring point position diagram.

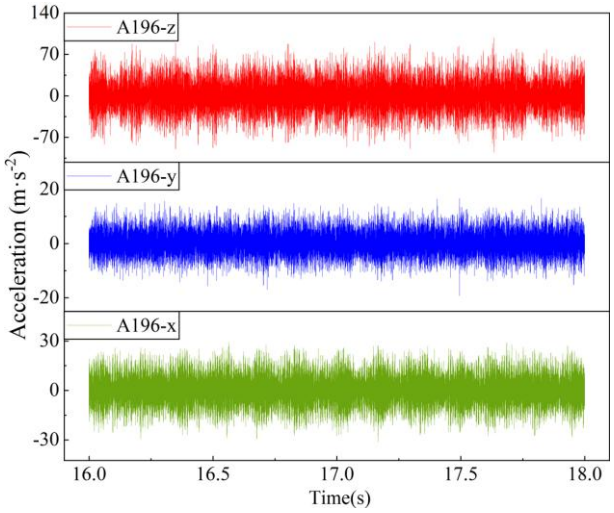

(a) Motor end cover

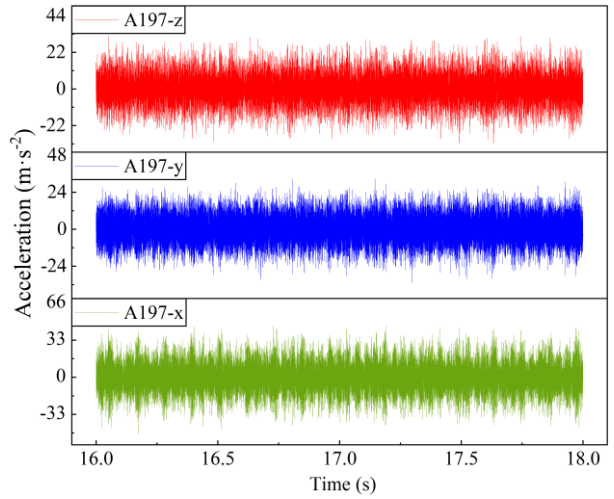

(b) Three-axis end

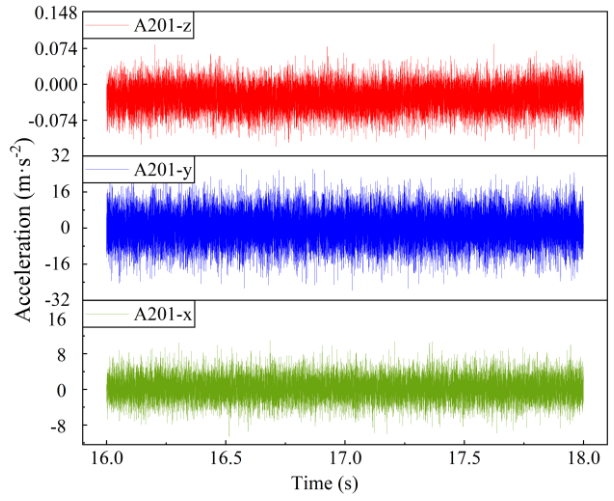

(c) Planetary gear train

Figure 3. Time domain vibration acceleration signals of different analog channels.

The vibration acceleration signal in the time domain can reflect the vibration level of the system to a certain extent. Figure 3 shows that at the three measuring points of the transmission test system of the shearer comprehensive test bench, the z-axis direction of the motor gear is the most intense, while the z-axis direction vibration acceleration value of the planetary gear train is small, that is, the gravity direction vibration level is low. Comparing the three positions comprehensively, the vibration at the end cover of the motor side is the most severe, followed by the three-axis end cover, and the vibration level at the planetary reducer is the lowest. The reason for the above phenomenon is that the input end is affected by the unbalanced magnetic pull of the motor, and the motor end cover is greatly disturbed. The three-axis assembly contains two gears, which are connected to the high-speed stage and the second-stage straight tooth transmission, including the most vibration frequency and the most complex vibration response. The planetary gear train has a compact structure and high density. The magnetic particle vibrator will have a certain support stiffness to the planetary gear train at the output end during the simulated cutting process, so the vibration in the gravity direction is not obvious.

2.1.2. Feasibility verification of simulation results

To investigate the comprehensive performance of the shearer gear transmission system under multi-field coupling and verify the feasibility and accuracy of the Romax simulation method for systematic vibration characteristic analysis, this paper takes the established physical test bench as the benchmark. The transmission system simulation model is constructed according to the structural form and actual parameters of the test bench to carry out dynamic comparison and verification. The transmission system structure is shown in Figure 4.

The simulation model adopts identical gear tooth configuration, structural layout, material properties and mechanical parameters as the test bench. The input operating conditions and external load conditions are unified, achieving consistency in geometric structure, material characteristics and loading boundary conditions. Based on this 1:1 full-parameter matching scheme, the simulation model maintains good consistency with the physical test bench in rotational speed, gear meshing frequency and constraint conditions. It lays a reliable foundation for the comparative analysis of numerical simulation and experimental results, and effectively improves the validity and verification credibility of the simulation model.

In the software, the gear material, bearing type, rotary shaft, lubricating oil and so on can be defined in detail. After the establishment of the gear-shaft-bearing model, it is necessary to import the finite element shell into the software, divide the shell into grids, and then define the material, contact and boundary conditions.

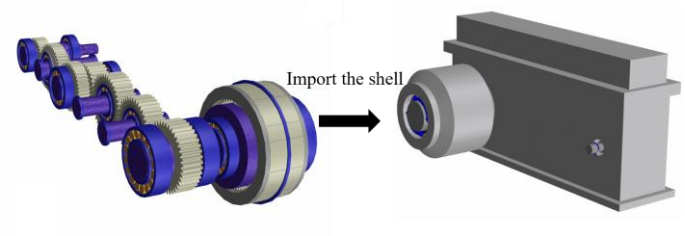

Figure 4. Romax test equipment 3D model.

Although the vibration acceleration data in the time domain reflect the vibration level of the system to a certain extent, it is not enough to reflect the vibration characteristics under different frequency components [22]. In order to more fully identify the vibration of the shell caused by the multi-order harmonic excitation of the gear in the frequency domain, the collected signal is subjected to fast Fourier transform. In the process of signal acquisition, in order to eliminate the extraction of gear meshing characteristic frequency by the frequency of other components, such as spline, magnetic powder brake, etc., the signal in the frequency domain is filtered. For the simulation model, the grid node is selected as the response point on the finite element shell. The selected position is consistent with the actual arrangement position of the acceleration sensor, and the three coordinates at the node are consistent with the sensor coordinates. The comparison between the two is shown in Figure 5. It should be clarified that the continuous spectrum obtained from Romax simulation is not a discrete FFT calculation result. The simulated continuous spectrum is essentially a fitted curve of vibration response peaks within the frequency band where meshing excitation energy is concentrated, generated by fitting the amplitude responses at various frequency points calculated by the system dynamics model. The physical meaning of the continuous spectrum is to comprehensively reflect the full-frequency vibration response trend of the transmission system housing and to clearly highlight the amplitude characteristics corresponding to the fundamental meshing frequency and its harmonics of each gear pair. In contrast, the experimental discrete spectrum is obtained by applying the Fast Fourier Transform (FFT) to the time-domain vibration signals collected by sensors, representing discrete amplitudes at finite frequency points. The simulated continuous spectrum characterizes the overall variation law of the vibration response, while the experimental discrete spectrum reflects the frequency-domain characteristics of actual measurements. The comparison between the two focuses on the consistency of dominant frequency distribution and amplitude variation trends, which can fully verify the accuracy and reliability of the Romax dynamics model.

The vibration acceleration curves from Romax numerical simulation are fitted curves of peaks in frequency bands with concentrated vibration energy. Figure 5 shows that most peak response points in sensor-collected data are close to the simulation curves, with consistent upward trends: At channel A196 (motor end cover), the first-stage gear pair's meshing frequency (346.27 Hz), its second harmonic (692.54 Hz), and the second-stage gear pair's fundamental meshing frequency (239.70 Hz) are all reflected in both tests and simulations, with the maximum frequency response amplitude in three directions at 950 Hz; At channel 197 (three-axis outer end cover), the x-direction at the second harmonic of the second-stage gear pair's meshing frequency (479.40 Hz) shows the highest vibration acceleration in both tests and simulations within the frequency range; At channel A201 (housing above the planetary gear train's inner ring gear), due to small z-direction vibration, test-simulation correspondence is poor in the 0-685 Hz low-frequency band, but good in x and y directions.

Compared with the acoustic full finite element method, the acoustic boundary element method not only avoids the waste of computing resources caused by large-scale calculation, but also accurately reflects the near-field acoustic radiation characteristics under the harmonic excitation factor of a certain level of gear pair, and solves the problem of infinite reflection and refraction of acoustic waves in a finite free field [23]. LMS Virtual.Lab multi-body dynamics analysis software can simulate the radiated noise of mechanical system by finite element method and boundary element method. Based on the simulation results, researchers can obtain various noise measurement data. Import the processed cutting part transmission system shell with vibration data into the software. After the acoustic grid is divided, when the special acoustic

solver is used to solve the problem, the grid quality requirements are not as high as those of the full finite element method.

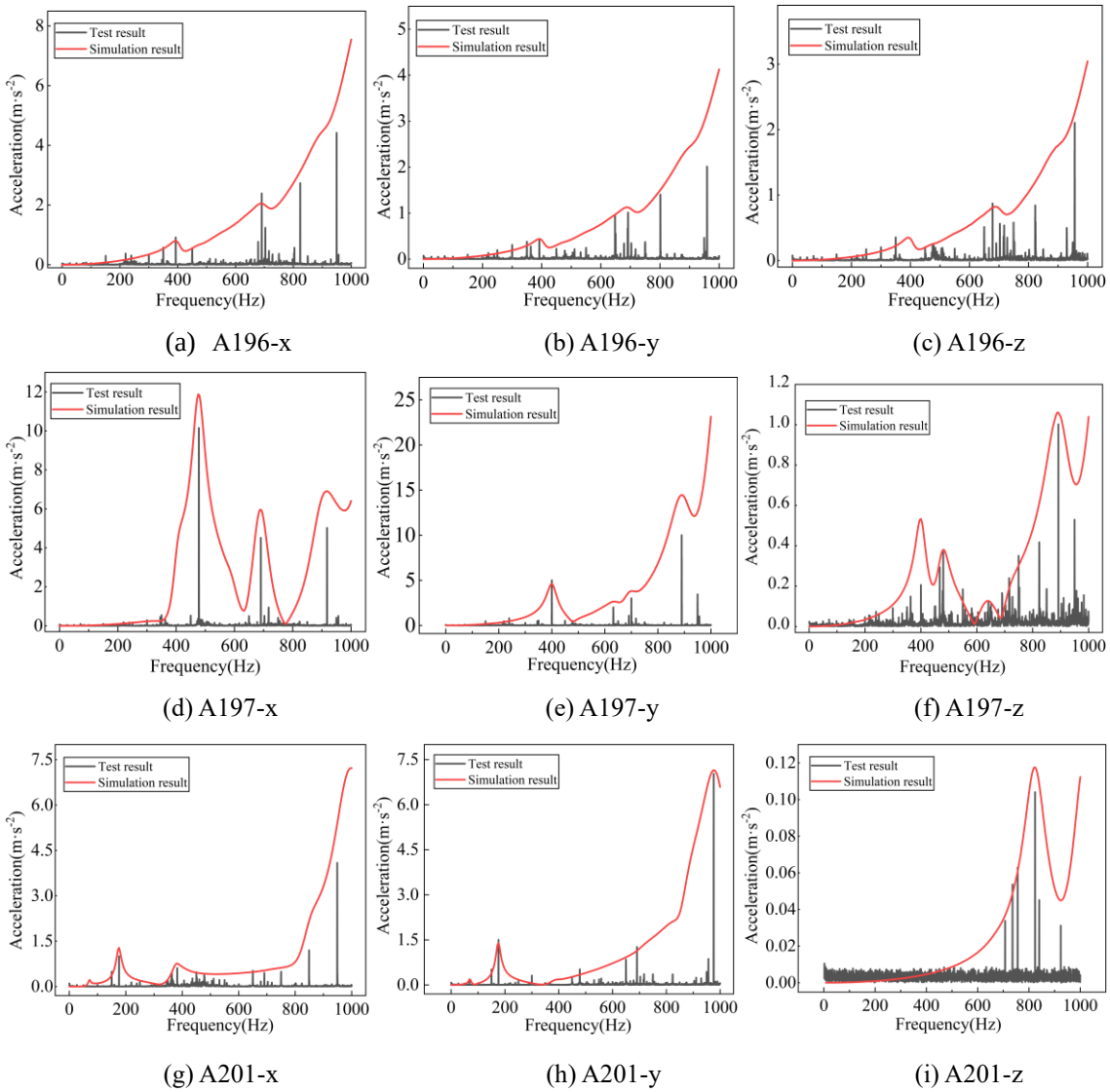

Figure 5. Simulation and experimental comparison of vibration at different measuring points under rated working conditions.

The grid size is:

$$L \le \frac{c_s}{6f_{max}} \tag{1}$$

Second-order unit size requirements:

$$L \le \frac{c_s}{3f_{max}} \tag{2}$$

Where c_s is the sound propagation speed under standard atmospheric pressure, the unit is m/s; f_{max} is the highest solution frequency.

The value of the target node is determined by the value of the source node:

$$P_{Target} = \frac{\Sigma_i^N \frac{P_i^{Source}}{d_i}}{\Sigma^N \frac{1}{d_i}} \tag{3}$$

Where P_{Target} is target grid vibration data, P_i^{Source} is structural grid vibration data. d_i is close to the distance between two nodes; N is the number of nodes.

Figure 6 presents noise comparison results: the microphone is actually 3 meters from the planetary gear train, with a 3-meter sound field established centered at its centroid in simulation. Within the 1000 Hz frequency response range, the maximum actual noise value differs little from the simulated one.

The error between the above results and simulations stems from vibration data acquisition being affected by multiple excitations. These include the motor's unbalanced magnetic pull at the input, the instantaneous impact of the magnetic powder brake, multi-order harmonics from involute spline meshing at the third and sixth axes, and noise acquisition not conducted in an anechoic chamber. Simulations do not account for the

equivalent effects of the motor, magnetic powder brake or splines. This results in fewer peaks and inaccurate fitting of peaks at corresponding frequencies. Despite these deviations, the error is within an acceptable range, verifying the reliability and accuracy of the Romax simulation method for the shearer cutting unit transmission system.

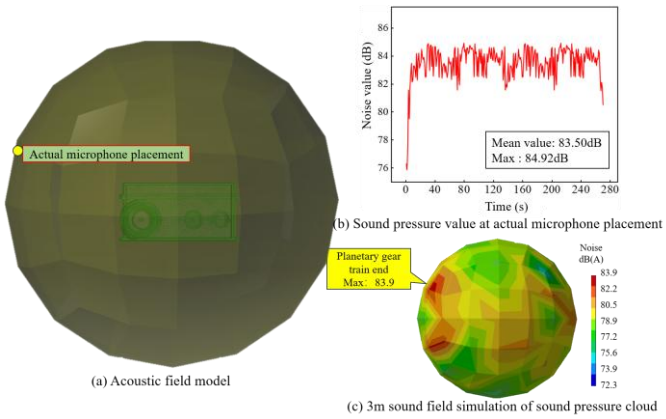

Figure 6. Comparison of noise test results and simulation results.

2.2. Dynamic model of MG2×250/1200-WD shearer cutting unit

2.2.1. Load model acquisition of cutting unit by Romax

In order to obtain the load characteristics of drum cutting coal rock, a nonlinear display dynamic model of drum cutting coal wall is established based on the existing literature[24,25] The establishment of the drum and the three-dimensional solid model are shown in Figure 7, and the diameter of the drum is Φ1400 mm×630 mm. In order to save time cost, the coal wall is set to 1800 mm×1800 mm×800 mm, the simulation time is set to 8s, and the traction speed is 6m/min. For pure coal and gangue-intercalated coal, the plastic kinematic constitutive model (MAT_PLASTIC_KINEMATIC) is adopted to accurately describe the elastoplastic deformation and fracture failure characteristics of coal and rock. According to the Protodyakonov coefficient criterion, the basic mechanical parameters of coal and rock materials are determined. For pure coal, the density is 1400 kg/m³, elastic modulus is 2.8 GPa, internal friction angle is 38°, and uniaxial compressive strength is 40 MPa. For gangue, the density is 2600 kg/m³, elastic modulus is 12.5 GPa, internal friction angle is 42°, and uniaxial compressive strength is 60 MPa. The drum and picks use the rigid material model (MAT_RIGID) with material 42CrMo to avoid structural deformation interference with load results during the cutting process. Meshing is performed using HyperMesh. Tetrahedral elements are selected for the complex geometries. The mesh size for the pick tips is set to 4 mm and 6 mm for the pick shank, while the single mesh size for the coal wall is set to 20 mm. During the LS-DYNA simulation, contact is established between the pick elements and the coal-rock elements. The picks are defined as the contact master surface, and the coal-rock mass as the contact slave surface. Contact failure and fragmentation between the picks and coal-rock are simulated using the surface-to-surface contact algorithm. To define this contact type, the keyword *CONTACT_ERODING_SURFACE_TO_SURFACE is employed. This algorithm not only simulates contact and interaction between an erodible surface and another body but also handles cases where material elements are deleted upon failure while contact continues between remaining elements. When contact stress exceeds the failure strength of the rock mass, linear strain occurs in the stressed elements, and the elements are automatically deleted once the strain exceeds the preset threshold. The keyword for applying non-reflecting boundary conditions in LS-DYNA is *BOUNDARY_NON_REFLECTING. To ensure the successful and accurate completion of the cutting process, correct boundary conditions must be applied. For the two lateral sides and the bottom surface of the coal block, which are not cut by the picks, full constraints are applied to these three surfaces using the keyword *BOUNDARY_SPC_SET.

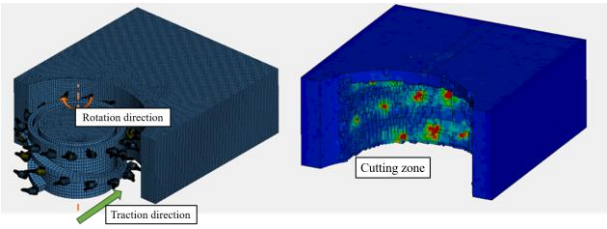

Figure 7. Simulation model of cylinder cutting coal wall.

Figure 8 is the time-varying torque on the drum obtained under the two loads of post-processing *f*4 pure coal and *f*4 coal evenly mixed with *f*6 gangue, which characterizes the instantaneous impact characteristics of the load during the cutting process. *f*4 indicates that the hardness is 4, and the compressive strength is 40 MPa. Comparing the two working conditions, it can be seen that the cutting of pure coal is compared under the condition of gangue. From the above

analysis, the two working conditions are about 0.6s, and the picks on the drum begin to contact the coal wall. Meanwhile, only a few picks first touch the coal wall and begin to bear a slight force. With the continuous traction of the drum, more and more picks contact the coal wall, and the force of the drum is also increasing, reaching the maximum value at about 2.1s. When the coal wall envelops the drum, the load torque fluctuates around a certain value, and the fluctuation effect is very signific.

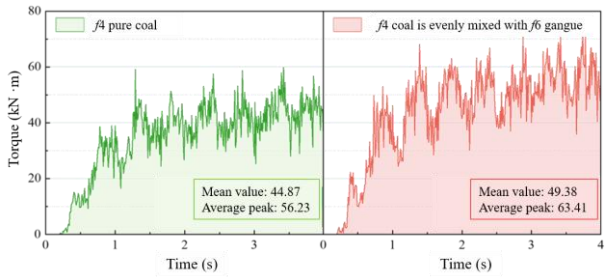

Figure 8. Time domain load torque diagram of spiral drum.

Through the time-varying drum load obtained in Ls-dyna, the peak average value, average value and average minimum value of the load after cutting the stable operation of different coal seams are counted, and several typical working conditions are generated, as shown in Table 2: working conditions 1 and 4 represent cutting light load conditions, working conditions 2 and 5 represent cutting rated conditions, and working conditions 3 and 6 represent cutting bad conditions. The load values in Table 2 'Romax Load Spectrum Conditions' are derived from LS-DYNA simulations. The load data is obtained from LS-DYNA simulations, and its statistical mean value is adopted to represent the cutting loads under different working conditions during actual operation. Based on these mean values, the corresponding input torques under each working condition are defined in Romax for subsequent dynamic simulation analysis.

Table 2. Romax load spectrum condition table.

Load processing	Numbering	Load torque (kN·m)
*f*4 pure coal	Condition one	36.73
	Condition two	44.87
	Condition three	56.23
*f*4 coal is evenly mixed with *f*6 gangue.	Condition four	40.82
	Condition five	49.38
	Condition six	63.41

2.2.2. Construction of dynamic model of cutting unit transmission system and near-field acoustic model

As a key component of coal mining equipment, the transmission system of shearer cutting unit not only reduces the speed and increases the torque, but also transports power for drum cutting coal. Its performance directly affects the production efficiency [26]. As shown in Figure 9(a), the transmission mode of the cutting unit transmission system is as follows: two mine-used flameproof three-phase asynchronous motors are connected in series as the input of power, which first flows into the three-stage straight teeth to decelerate, and then passes through the first-stage NGW planetary gear train to the cutting drum. The total transmission ratio is 31.48. In the first-stage straight tooth transmission, the cutting motor is connected in series by two idlers, and the transmission ratio is 1.762. The modulus of the secondary straight tooth is increased to meet the design requirements, and the transmission ratio is 1.682. The three-stage straight tooth deceleration increases the transmission distance by two idlers to meet the requirements of the mining height of the shearer, and the transmission ratio is 2.15. The transmission ratio of planetary reducer is 4.941. In the established dynamic model of the shearer cutting unit transmission system, the basic geometric parameters of each gear pair are determined according to the actual design drawings of the shearer cutting unit, including module, number of teeth, pressure angle. The transmission distribution table at all levels is shown in Table 3. All gears are made of 18Cr2Ni4WA steel with surface hardening treatment, a surface hardness of 280 HB, elastic modulus of 207 GPa, and Poisson's ratio of 0.3. All shaft segments are isotropic with a Young's modulus of 207 GPa, density of 7800 kg/m³, and Poisson's ratio of 0.29. All critical shafts were flexibilized to establish a rigid-flexible coupled model. The lubricant adopts ISO standard VG320, and the oil level height is set to the horizontal plane at the coordinate origin. The bearings employed in the model are all standard industrial bearings from SKF. The specific models, types and installation positions are listed in Table 4.. Bearing models are selected according to the actual assembled bearings of the shearer. Bearing stiffness is calculated using the rolling element load distribution formula and Hertzian contact stiffness theory, and the values comply with ISO standards and bearing handbooks. The housing was meshed in Hypermesh. Tetrahedral elements were used for preprocessing the complex flexible body. The mesh consists of 439,201 tetrahedral elements and 1,038,888 nodes. In Abaqus, the housing material was set as isotropic with

a Young's modulus of 175 GPa, Poisson's ratio of 0.3, and density of 7823 kg/m³, and the material properties were assigned to the mesh file. Regarding boundary conditions, the rocker arm hinge joint was simplified using a rigid fixed constraint and imported into Romax as a flexible component. Finally, the imported flexible components were connected to rigid components via node-to-node connections.

Romax software is used to establish the dynamic model of the dual-motor cutting transmission system as shown in Figure 9(b). The parametric modeling function of the gear can define the actual tooth thickness of the gear in detail according to the length of the common normal line or the span ball (rod) distance. The center distance between gears and their upper and lower deviations are determined by defining the position of each axis. Its bearing library contains detailed three-dimensional models provided by bearing manufacturers such as SKF and FAG, and accurately calls rolling bearings to complete accurate modeling of cutting unit bearings. The shell is divided into grids, and the material properties and other boundary conditions are defined.

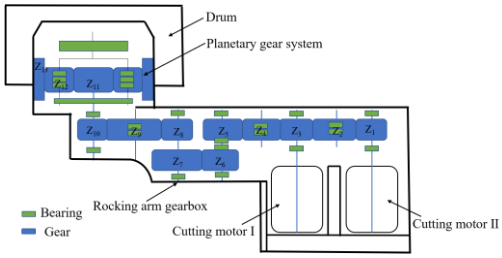

(a) Cutting unit transmission system diagram

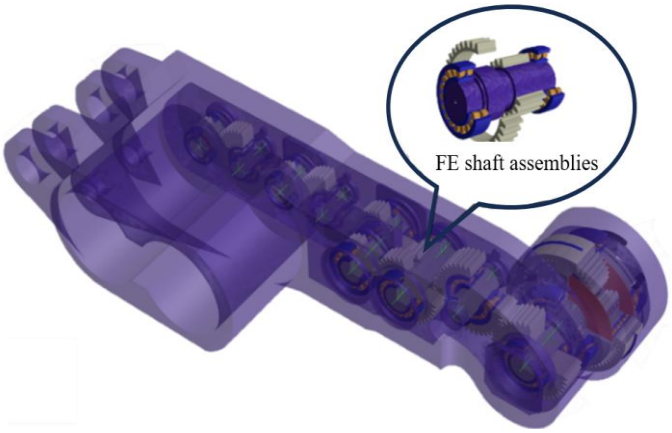

(b) Romax dynamic mod

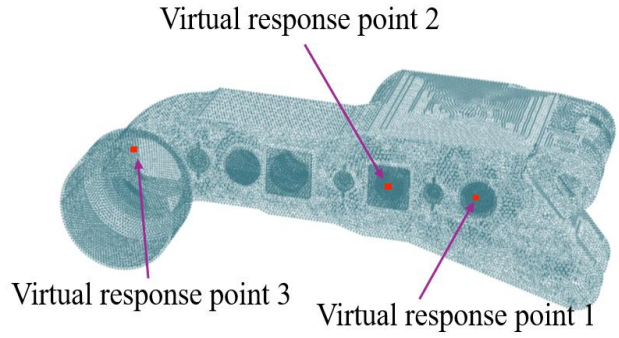

(c) Shearer rocker arm gear box virtual measuring point location diagram

Figure 9. Cutting part drive system schematic and dynamic model.

Table 3. Gear transmission distribution table at all levels of cutting section.

Number	Z_1	Z_2	Z_3	Z_4	Z_5	Z_6	Z_7	Z_8	Z_9	Z_{10}	Z_{11}	Z_{12}	Z_{13}
Quantity	1	1	1	1	1	1	1	1	1	1	1	4	1
Number of teeth	21	44	22	44	37	22	37	20	39	43	17	25	67
Rotational speed	739	352	739	352	419.4		249.4		127.9	116.0		23.4	0
Rotational frequency	12.3	5.8	12.31	5.88	6.99		4.16		20.3	1.93		0.39	0
Module			7		8				8			7	
Transmission ratio			1.762		1.682				2.15			4.941	
Mesh frequency			219.63		153.78				83.13			32.64	
pressure angle					20°								

Table 4. Relevant parameters of bearings at each stage.

Bearing position	Bearing type	Bearing designation	Bearing position	Bearing type	Bearing designation
Bearing at shaft 1	Cylindrical roller bearing	NJ2218EC	Bearing at shaft 7	Cylindrical roller bearing	NJ321EC
Bearing at shaft 3	Cylindrical roller bearing	NJ2218EC	Bearing at shaft 8	Cylindrical roller bearing	NJ224EC
Bearings at shafts 2 and 4	Cylindrical roller bearing	NJ316EC	Right bearing of planet carrier	Tapered roller bearing	32056X
Bearing at shaft 5	Cylindrical roller bearing	NJ221EC	Bearing for planet gear pin	Spherical roller bearing	22311E
Bearing at shaft 6	Spherical roller bearing	22222E	Left bearing of planet carrier	Tapered roller bearing	32048X

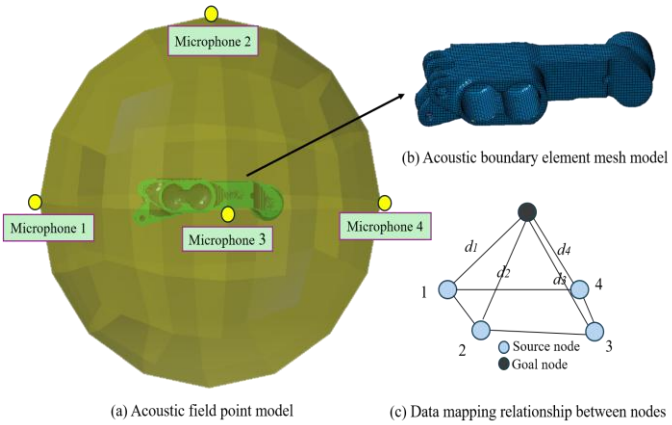

Figure 10. Virtual microphone space layout diagram and Acoustic field point model.

In order to further explore the noise radiation of each azimuth on the fully mechanized mining face when cutting different coal seams, a virtual microphone is arranged in three-dimensional space to evaluate the noise radiation characteristics under two working conditions. According to the simulation requirements, the acoustic response within the maximum frequency range of 2000 Hz is calculated, and the mesh size is determined to be 30 mm based on Equations (1) and (2). As shown in Figure 10(a) the virtual microphone space layout diagram. The established acoustic boundary element grid model is shown in Figure 10(b), in which the number of grid elements is 131198, the number of nodes is 65583, and the 3 m free field is set. Acoustic boundary element method is used to simulate the radiation noise of the cutting part. The vibration data of the shell obtained from the vibration analysis are transferred to the acoustic boundary element model established previously. The vibration displacement data of the rocker gearbox shell are better applied in the established acoustic boundary element model.

3. Dynamic characteristics analysis of transmission system of shearer cutting unit

3.1. Coupling modal analysis of cutting unit transmission system

The shearer cutting unit is prone to vibration, noise and even resonance due to large instantaneous load impact and complex frequency components. Thus, studying the modal characteristics of its transmission system is crucial for improving equipment stability and production efficiency. Modal analysis characterizes the inherent vibration properties of mechanical structures, which are defined by natural frequencies (each matching a specific mode shape) and eigenvectors. These modal parameters require cross-validation through theoretical analysis and operational modal tests under environmental excitation to optimize the dynamic performance of the transmission system [27]. There are two ways to obtain the cutting unit's modal: Using an exciter or force hammer as the excitation source for frequency sweeping, and arranging vibration sensors at key positions to collect resonance frequencies; Solving theoretical values via finite element software [28]. For the rocker arm reducer, the shaft rotation generates large centrifugal force, so when calculating its rotating modal with Romax, the nonlinear perturbation modal analysis with rotational softening should be adopted. The cutting unit's transmission system has infinitely many modals. Higher-order modes are mostly integer superpositions of lower-order ones and have little impact on actual structural vibration, so low-order modes are the focus in engineering. Meanwhile, the natural frequency of the maximum coupled modal should cover the concerned frequency range.

Table 5 is the modal natural frequency table. Considering the influence of the fundamental frequency of the excitation frequency and its frequency doubling on the transmission system, according to the rotation frequency of each shaft and the meshing frequency of the gear pair calculated in the transmission distribution table of each level in Table 3, the several order modal shapes are shown here. The modal identification of the cutting unit transmission system is carried out, and the motion information and natural frequency of all node coordinates are obtained in the modal space, which lays a foundation for the study of system resonance. Romax simulation software is used to extract the first 40 modes of the gearbox of the front cutting part. In order to show the main vibration modes, normalization is done here, as shown in Figure 11. Through systematic comparative analysis, the resonance risk of the transmission system is explicitly evaluated. It can be concluded from Table 6 that all excitation frequencies are effectively separated from the adjacent natural frequencies, and thus no resonance risk exists in the system.

Figure 11 shows the several order vibration modes of the gear transmission system of the cutting part that are prone to resonance. It can be seen from the modal analysis results that

there is no offset amplitude on the main vibration mode shell of the first seven modes, which is the axial movement of the gear shaft and the idler wheel. At this time, the stiffness of the shell is much greater than that when resonance occurs. Starting from the eighth order mode, the vibration of the rocker arm shell caused by the high kinetic energy of the transmission system appears on the shell, which is manifested by the coordinated vibration of multiple components, and the vibration mode is becoming more and more complex. The shell offset is the most obvious in the ninth and tenth order modes, and the amplitude offset is concentrated in the planetary reducer part. The first, seventh, eighth and fifteenth order resonance modes of the input end of the transmission system are the first, seventh, eighth and fifteenth order. The first, seventh and eighth order of the two motor gear shaft components have the largest offset amplitude, and the maximum amplitude offset of the fifteenth order appears on the idler wheel. The obvious several-order modes of the intermediate gear assembly of the transmission system are the fifth, sixteenth and eighteenth orders, and their maximum values appear on the five-axis assembly, the six-axis assembly and the seven-axis idler assembly respectively. The larger modes of the planetary reducer of the transmission system are the ninth, tenth and nineteenth orders, and the vibration modes are mainly manifested in different forms of torsion and offset.

Table 5. Natural frequency table of the first 40 modes.

Order	Frequency (Hz)	Order	Frequency (Hz)	Order	Frequency (Hz)	Order	Frequency (Hz)
1	4.7	11	142.5	21	359.7	31	600
2	4.9	12	174.4	22	373.5	32	613.7
3	4.9	13	180.1	23	386.1	33	619.8
4	5.0	14	218.8	24	423.9	34	649.7
5	6.3	15	223.9	25	432.7	35	652.6
6	7.5	16	269.0	26	461.7	36	663.6
7	7.6	17	281.1	27	508.3	37	676.1
8	25.7	18	304.7	28	524.1	38	693.5
9	57.4	19	323.5	29	564.6	39	698.5
10	65.9	20	342.6	30	569.7	40	701.1

Table 6. Comparison between excitation frequencies and natural frequencies.

Excitation Type	Excitation Frequency (Hz)	Nearest Natural Frequency (Hz)	Excitation Type	Excitation Frequency (Hz)	Nearest Natural Frequency (Hz)
Shaft Rotation Frequency	0.39	4.7	3rd-stage Meshing Frequency	83.13	65.9
Shaft Rotation Frequency	5.80	4.9	Planetary-stage Meshing Frequency	32.64	57.4
Shaft Rotation Frequency	6.99	7.5	1st-stage Meshing 2nd Harmonic	439.26	423.9
Shaft Rotation Frequency	12.31	25.7	2nd-stage Meshing 2nd Harmonic	307.56	304.7
2nd-stage Meshing Frequency	153.78	142.5	3rd-stage Meshing 2nd Harmonic	166.26	174.4

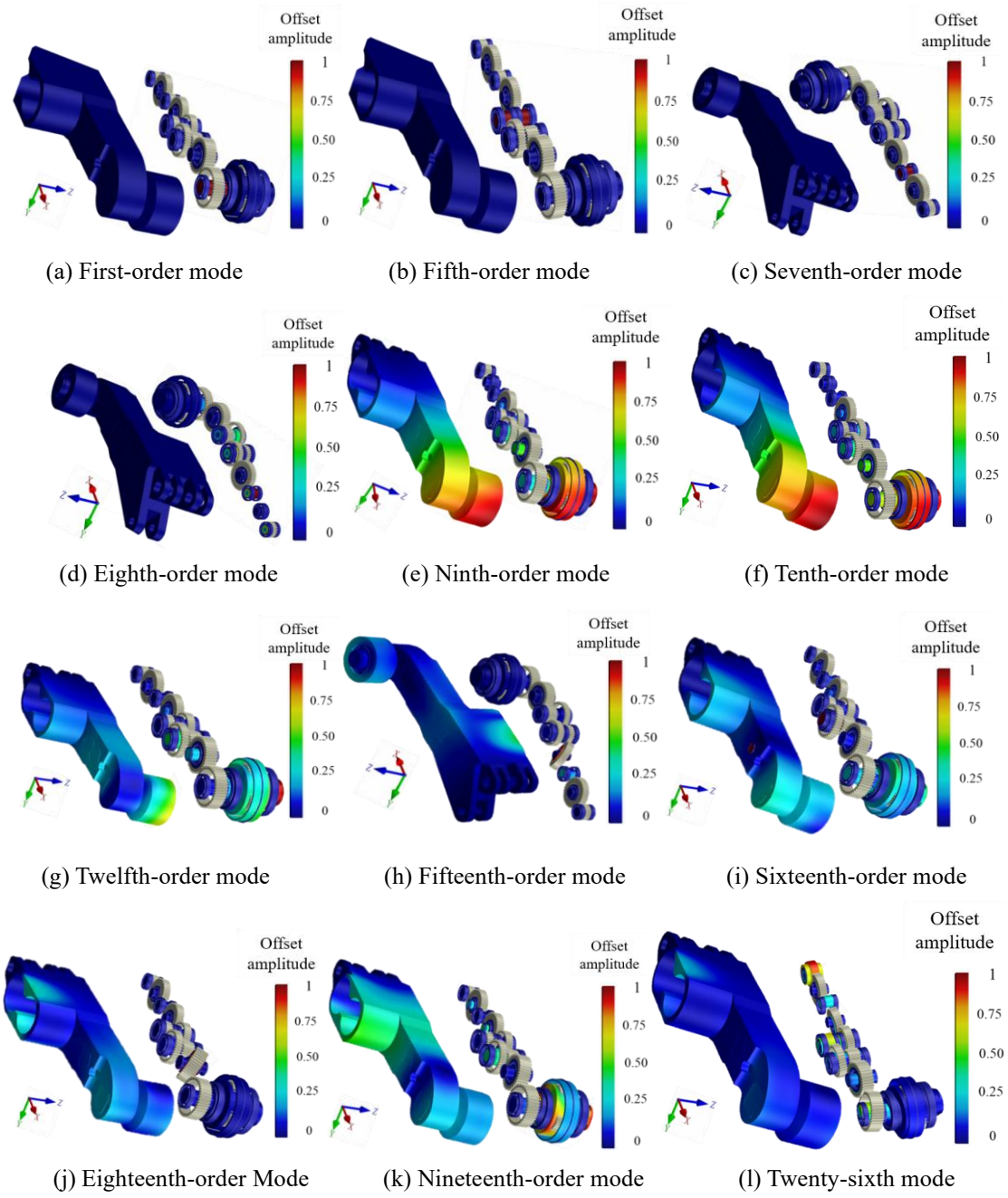

(a) First-order mode (b) Fifth-order mode (c) Seventh-order mode

(d) Eighth-order mode (e) Ninth-order mode (f) Tenth-order mode

(g) Twelfth-order mode (h) Fifteenth-order mode (i) Sixteenth-order mode

(j) Eighteenth-order Mode (k) Nineteenth-order mode (l) Twenty-sixth mode

Figure 11. The main modes of the cutting part drive system of modal analysis.

3.2. Vibration response analysis of homogeneous coal seam and gangue coal seam under extreme conditions

Based on the modal analysis results that the system has no resonance risk, the vibration response characteristics of the transmission system under extreme working conditions are further analyzed in the following section. Previous studies have confirmed that the first three-order harmonic components of gear transmission error (TE) are the dominant contributors to system vibration energy, while the influence of high-order harmonics above the third order is negligible and can be excluded from the analysis [29]. In this study, the extreme working condition of homogeneous pure coal seam corresponds to Condition 3 in Table 2, and the extreme working condition of gangue-intercalated coal seam corresponds to Condition 6. To investigate the influence of harmonic excitation induced by gear meshing on the system vibration behavior under the above harsh cutting conditions, fast Fourier transform (FFT) was performed on the time-domain TE signals of the high-speed motor gear pairs and the planetary gear train. Quantitative analysis of the first three-order harmonics of each gear pair was conducted to identify the dominant vibration excitation sources, which provides a theoretical basis for targeted vibration suppression

optimization and improvement of the system vibration reliability.

Figure 12 shows the harmonic peak of the axial transmission error after fast Fourier transform, which takes into account the flexibility of the shaft and the deviation of the tooth thickness of the gear. When the gear transmission system of the cutting part cuts the gangue coal seam, due to the greater load torque, the amplitude of each order harmonic of each gear pair in the frequency domain is larger than that of the pure coal. The motor gears Z1 and Z2 are both located in the high-speed level. Although their transmission errors are different in the angle domain, the results are the same after conversion to the frequency domain, and the first-order harmonic amplitude is higher than the second and third-order harmonic contributions. The planetary reducer has a large transmission ratio, compact structure and high energy density. The harmonic amplitude in the frequency domain is significantly smaller than that of the straight tooth transmission. In the process of planetary gear transmission, although the curves in the angle domain are roughly the same, the harmonic amplitude is the largest when the planetary gear is rotated to the 180° position in the frequency domain, followed by the 90° phase angle position, the 270° phase angle, and the 0° position. The amplitude is the smallest, but the contribution of the second-order harmonic to the transmission error of the gear pair is the largest.

The vibration response of the transmission system is mainly manifested as the dynamic contact force of bearings, the displacement and acceleration response of the housing, and the vibration energy is transmitted to the shearer rocker arm housing through the bearing support system. Under both homogeneous and gangue-intercalated working conditions, the bearings operate at high speed under alternating loads, and system vibration may induce lateral displacement of the rolling elements relative to the inner and outer rings, resulting in non-uniform stress distribution on the bearing raceways. To analyze the dynamic force and acceleration response of the shearer cutting unit in the frequency range of 0–2000 Hz, dynamic condensation was performed on the finite element model of the housing, and the dynamic characteristics of the housing were solved in combination with the speed fluctuation of high-speed gears under transient impact excitation during the cutting process.

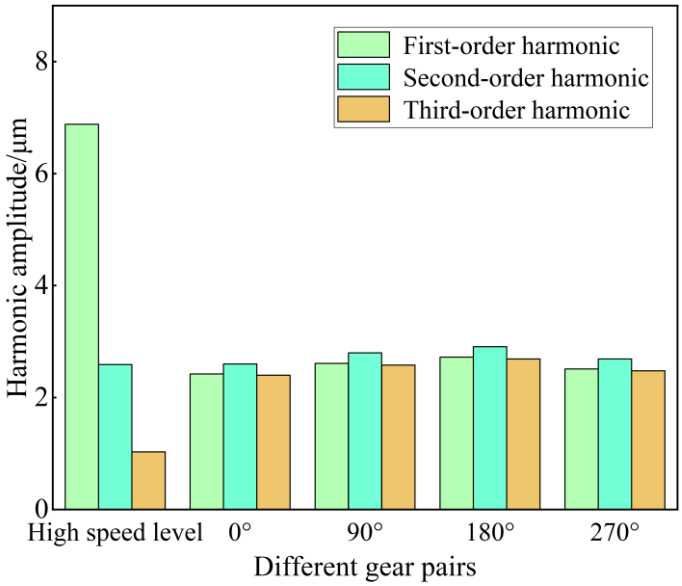

(a) homogeneous coal seam

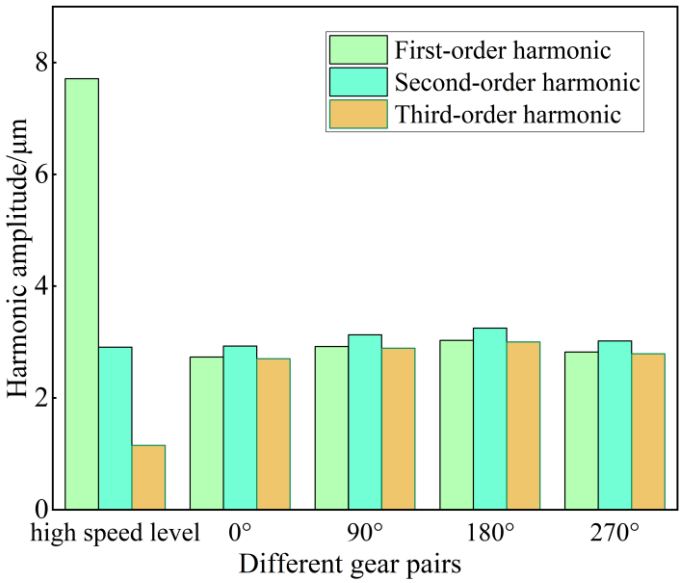

(b) gangue coal seam

Figure 12. Harmonic amplitude of gear pair transmission error under different working conditions.

Firstly, the response analysis of the force response at the bearing is carried out. Figure 13(a) shows the contact force response of the bearing in the frequency domain of the transmission system under high-order frequency excitation. Observing the dynamic response results of each bearing hole in the frequency domain, it can be seen that as the frequency increases, the force of the bearing under the influence of multiple harmonics will increase. There are multiple peaks under the influence of multiple harmonics of the high-speed stage gear. The corresponding frequency is the double frequency of the meshing frequency of the first-stage gear pair: 439.26 Hz, and the other higher-order frequencies:1153.36 Hz,

1247.97 Hz. At 1247.97 Hz, the peak value of the dynamic contact force of the two supporting bearings in the one-axis assembly exceeds that of the five-axis bearing. Combined with the natural frequency of the system, the possibility of resonance is avoided. When the excitation frequency reaches 1600 Hz, although the bearing force will continue to increase, considering that the excitation frequency and its frequency doubling of the shearer rocker arm service environment are difficult to reach this level, so there is no in-depth study.

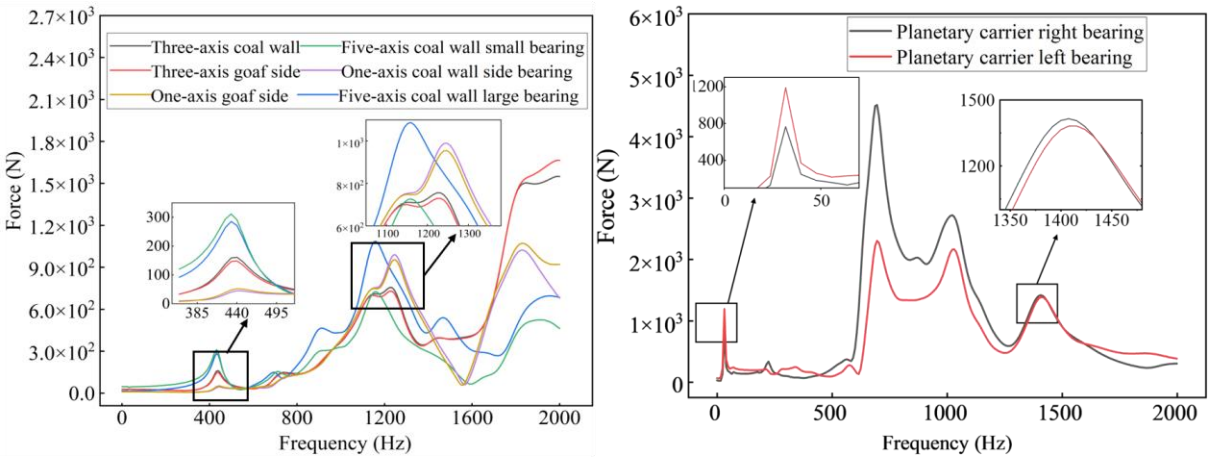

(a) High speed bearing force response

(b) Bearing force response at the planetary frame

Figure 13. Force response under pure coal limit condition.

From the perspective of bearing load conditions, motor gear Z1 — the farthest from the load in the transmission chain — runs at high speed but bears low load, so the first shaft's bearings endure the least force. Motor gear Z3 carries power from gear Z1 and the three-phase motor; it also endures load forces, making the third shaft assembly's bearings have the second-least force. The fifth shaft assembly has a relatively high failure rate in actual fully mechanized mining faces; simulations show its bearing bears the most force among high-speed stage bearings. This shearer adopts a mine-used flameproof motor. The eight-pole asynchronous motor has lower input speed and system input frequency than the four-pole version, making the driver motor more reliably adaptable in terms of vibration. Multi-order harmonic excitation is used to evaluate the planetary gear train's vibration level, with the response force at the planet carrier's support bearing reflecting this level to some extent.

Figure 13(b) shows the dynamic force response curve of the planetary carrier bearing under the harsh working conditions of pure coal. Compared with the bearing in the high-speed stage assembly, the dynamic force at the planet carrier bearing is larger. The right shaft end of the planet carrier is directly connected to the spiral drum, and the load effect is more significant. In the frequency range of 0-2000 Hz, the force response amplitude is larger than that of the left bearing of the planet carrier. With the increase of the excitation frequency, the force response amplitude at each bearing has four obvious peaks, and the corresponding frequencies are 32.64 Hz at the meshing frequency of the planetary gear train, 696.61 Hz at the high-order excitation frequency, 1024.02 Hz at the high-order excitation frequency, 1408.47 Hz at the high-order excitation frequency. Under this harsh working condition, the dynamic response force amplitude of the right bearing of the planet carrier is the largest, and its maximum value reaches 4516.6 N. Secondly, the acceleration response of the virtual sensor on the shell surface is analyzed. Although the vibration effect of the bearing on the transmission path is more direct, it is not easy to observe. Due to the high frequency of faults in the service process of the two motor gears and the planetary gear train, in order to more intuitively evaluate the vibration level of the rocker gear box, the acceleration response point is established on the surface of the box, and the vibration amplitude of the x, y and z directions at the response point is observed, as shown in Figure 9(c). In the following, the vibration correlation analysis is based on three virtual measurement response points.

The virtual response point 1 and 2 are located at the end

cover of the coal wall of the motor gear shaft, respectively, to evaluate the shell response under multiple excitations of high-speed gears. The virtual response point 3 is located directly above the inner gear ring, which is used to evaluate the acceleration response level of the planetary reducer under complex excitations such as sun gear and planetary gear, planetary gear and inner gear ring. Through the dynamic vibration analysis of the system, the acceleration amplitude at three response points under the limit condition of cutting pure coal is obtained, as shown in Figure 14.

As shown in Figure 14(a) and (b), under the extreme condition of cutting pure coal, virtual measuring points 1 and 2 are subjected to multi-order harmonic excitation at the high-speed stage. The vibration in the y-direction (gravity direction) accounts for a large proportion in the vector acceleration synthesis with high amplitude, while the vibration amplitudes in the x-direction (shearer traction direction) and z-direction (axial direction) are smaller. The high-order frequency responses of the two points show two significant peaks at 1247.97 Hz and 1792.48 Hz. At the end cover of motor gear Z1, the peaks are 23.921 and 22.408 $m \cdot s^{-2}$, so the former is more responsive; at the end cover of Z3, the peaks are 17.069 and 27.605 $m \cdot s^{-2}$, so the latter is less responsive. Additionally, the high-frequency axial acceleration amplitude at the second shaft end cover near motor gear Z2 is excessively large. In Figure 14(c), the vibration response of the planetary reducer assembly is lower than that of the high-speed stage. At 3× the meshing frequency of the high-speed stage (654.48 Hz), the amplitudes in the gravity direction and traction direction account for a larger proportion in the acceleration vector synthesis, and the maximum acceleration is 13.442 $m \cdot s^{-2}$. After confirming the main frequencies and peaks, it is shown that the shearer's vibration during homogeneous coal cutting is normal, which provides a reference for vibration mode identification and fault detection.

In order to explore the frequency response characteristics of the gear transmission system of the cutting part when cutting the gangue coal seam, the dynamic contact force between the high-speed bearing and the planetary carrier bearing in the range of 0-2000 Hz is extracted. Firstly, the dynamic contact force at the bearing is analyzed.

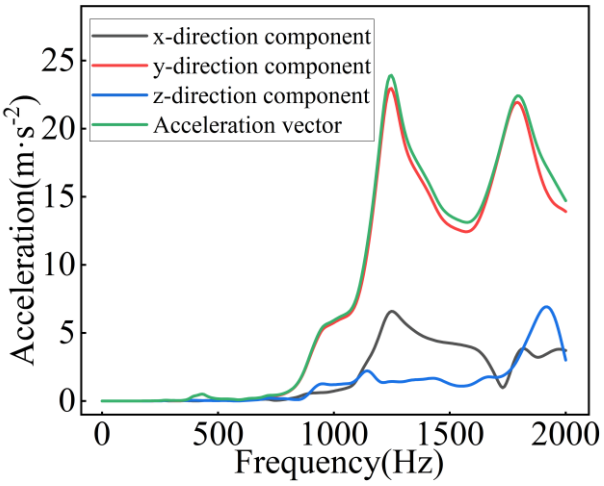

(a) Virtual point 1

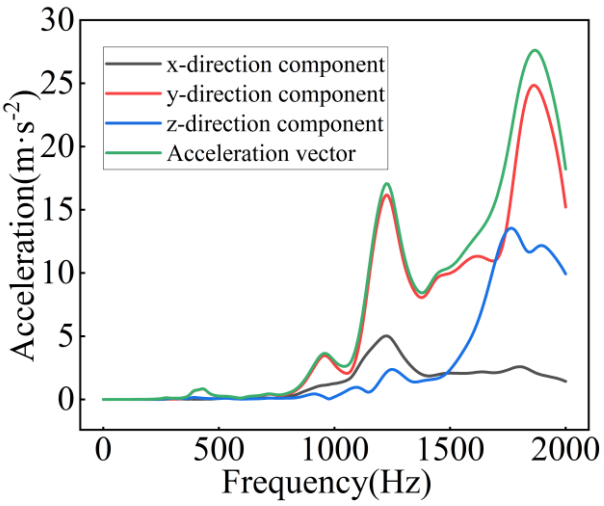

(b) Virtual point 2

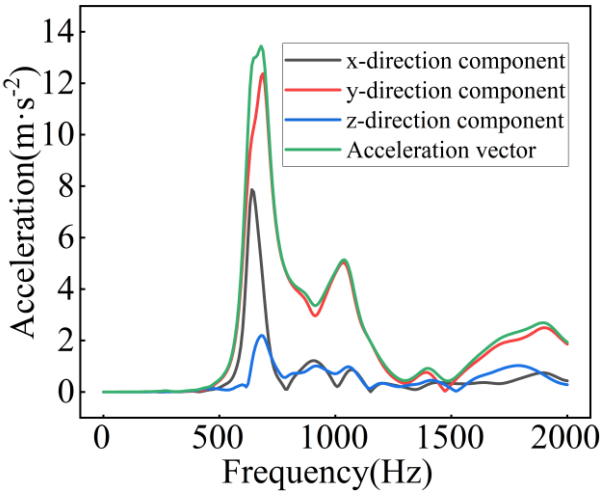

(c) Virtual point 3

Figure 14. Acceleration amplitude at each virtual measuring point.

Figure 15 (a) shows the dynamic contact force response amplitude of the high-speed bearing under the limit working condition of the shearer cutting the gangue coal seam.

Compared with the limit condition of cutting pure coal, the peak value of dynamic response force at each bearing is significantly improved, but the peak waveform and corresponding frequency do not change much. In the range of 0-500 Hz, the peak value of the dynamic response force of the two bearings on the five-axis coal wall side is larger than that of the other four bearings, and the corresponding frequency is the double frequency of the first-stage gear pair. There are two response peaks in the range of 1100-1360 Hz, and the corresponding frequency is consistent with the above. The peak response of the five-axis coal wall side bearing is the largest, and the corresponding peak of the one-axis coal wall side bearing is the second. Therefore, for the straight tooth transmission of the cutting part, the dynamic contact force response peak at the bearing is directly related to the load. When cutting the gangue coal seam, the response peak force generated by the bearing due to vibration is larger than that when cutting pure coal.

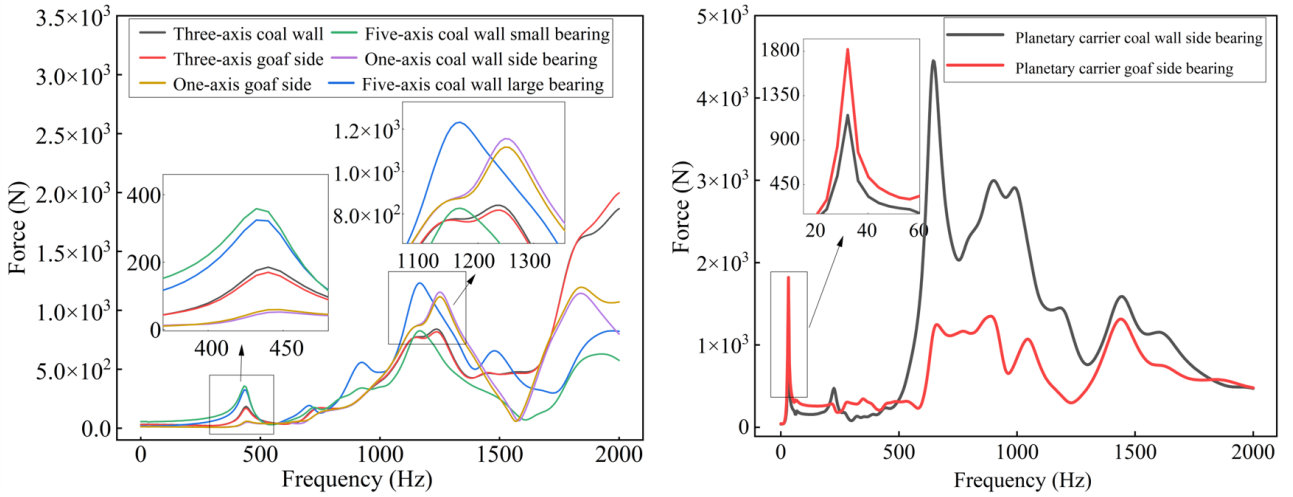

(a) High speed bearing force response

(b) Bearing force response at the planetary frame

Figure 15. Force response under the limit condition of mixed gangue.

Figure 15(b) shows the dynamic contact force response amplitude curve of the two bearings at the planet carrier under the limit working condition of the cutting part of the shearer. Under this condition, the amplitude of the bearing response force at the planetary reducer is larger than that of the cutting homogeneous coal seam, and there are more wavelet peaks, and the bearing force of the gangue condition is more complex. At the meshing frequency of the planetary gear train of 35.64 Hz, the peak value of the dynamic response force of the goaf side bearing of the planet carrier is larger than that of the coal wall side. At 473.29 Hz, as the excitation frequency continues to increase, the response level of the bearing on the coal wall side of the planet carrier exceeds that on the goaf side, and the vibration on the planet carrier is mainly the vibration of the bearing on the goaf side. At the excitation frequency of 696.61 Hz, the peak response difference between the two bearings is larger than that when cutting pure coal. When the excitation frequency exceeds 1408.47 Hz, the dynamic contact response force of the bearing tends to decrease.

Secondly, the acceleration response at the virtual measuring point is analyzed. When the gangue coal seam is cut, although the response force amplitude at the bearing is greatly improved, from the perspective of the transmission path, the final shell vibration response is greatly affected by the multi-gear harmonics. In order to further explore the acceleration response of the gear transmission system of the cutting part under the working condition of the parting, the response amplitude of the acceleration and its components is extracted at the virtual measuring point shown in Figure 9(c). By comparing the response acceleration under different working conditions, it can not only evaluate the vibration level of the rocker gearbox, but also has certain reference significance in the identification of vibration mode.

Figure 16 shows the amplitude responses of acceleration and its components at three virtual measuring points under extreme conditions when cutting gangue-intercalated coal seams. The acceleration peaks at the three virtual measuring points are significantly higher than those under the extreme condition of

cutting pure coal, indicating a more intense vibration level. At virtual measuring point 1 and 2, the vector amplitudes of acceleration reach their maximum values at 1247.97 Hz and secondary maximum values at 1792.48 Hz, which are 29.321 $m \cdot s^{-2}$ and 24.584 $m \cdot s^{-2}$ respectively. At the same measuring point, the vibration amplitude of the housing along the y-axis is more intense, as shown in Figure 16 (a) and (b). At virtual measuring point 3, due to the excessive load on the drum, as the excitation frequency increases, the amplitude in the high-frequency response range of 1000–2000 Hz still shows an upward trend with numerous small peaks. Therefore, the vibration level under the gangue-intercalated coal seam condition is higher and the response is more complex than that under the homogeneous coal seam condition: the amplitude of the dynamic contact force response at the bearings is higher; the vibration of the housing surface not only has higher peaks, but also more small peaks appear in the high-frequency response range as the transmission system is subjected to more severe forced vibration.

The above results indicate that the vibration level under the gangue-intercalated coal seam condition is significantly higher and the response characteristics are more complex than those under the homogeneous coal seam condition: the amplitude of the dynamic contact force response at the bearings is higher, and the housing surface vibration not only has higher main peaks, but also presents more secondary peaks in the high-frequency response range due to the more severe forced vibration of the transmission system. Based on the dynamic model of the cutting unit transmission system, the simulation results of the bearing dynamic contact force and the housing acceleration response under the two extreme working conditions show that the dynamic contact force of the bearings on the coal wall side of the fifth shaft assembly is the most prominent in the high-speed stage, while the dynamic contact force of the coal wall side bearing of the planet carrier is the highest in the planetary reducer. The characteristic frequencies corresponding to the main peaks of the high-speed stage are the second harmonic of the high-speed stage meshing frequency and the meshing frequency of the planetary gear train; at the virtual measuring points, the vibration acceleration is the highest in the gravity direction, and the eight-pole asynchronous motor exhibits better vibration adaptability than the four-pole motor.

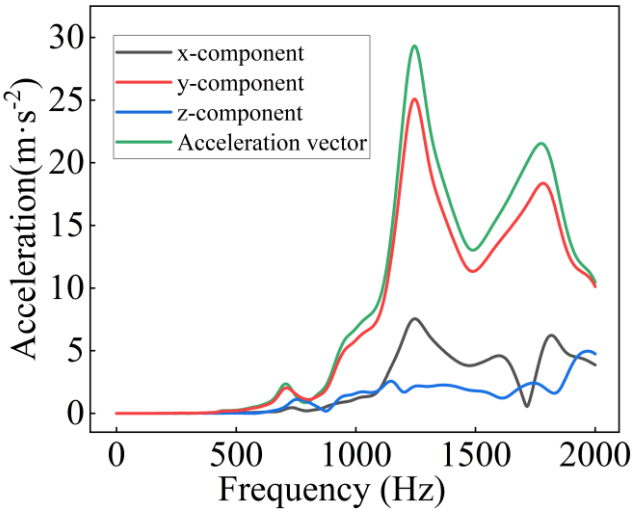

(a) Virtual point 1

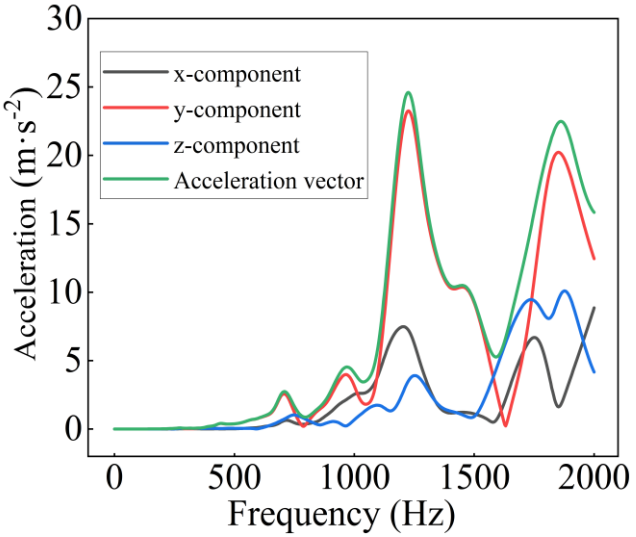

(b) Virtual point 2

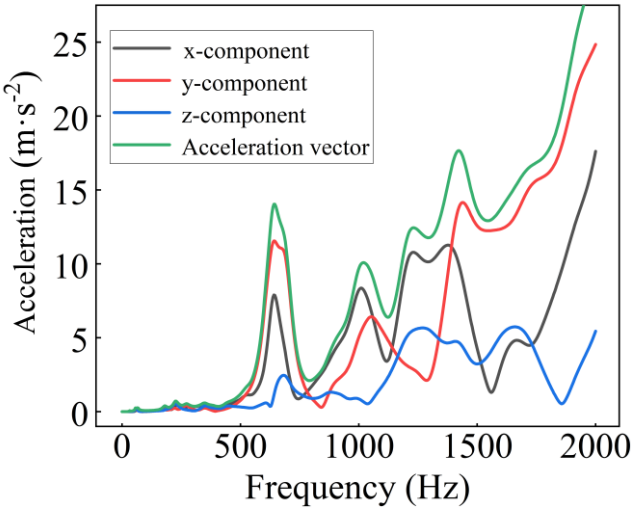

(c) Virtual point 3

Figure 16. Acceleration response under the limit condition of mixed gangue.

3.3. Noise response analysis of homogeneous coal seam and gangue coal seam under extreme conditions

Vibration excitation is the core source of gearbox radiated noise. Based on the vibration response law of the transmission system under different working conditions, the noise radiation characteristics of the cutting unit are further analyzed in this section. In the previous paper, the vibration response of the gear transmission system of the cutting unit under the homogeneous coal seam was explored. The radiation noise not only worsens the working environment and reduces the bearing reliability of the equipment, but also causes harm to the physical and mental health of workers in the high-decibel environment. On the transmission path, the shell, as an important part of the noise propagation process, stores a lot of information of the internal excitation, and acts on the surrounding air flow field until it propagates to the receiver sound source [30]. In order to obtain the sound field radiation effect under the cutting limit condition, the simulation analysis is carried out in LMS virtual.lab to explore the characteristics of sound field radiation.

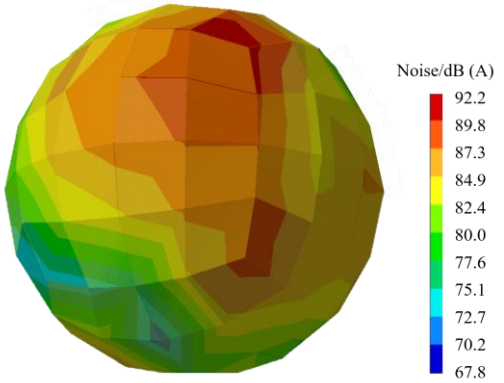

(a) Homogeneous coal seam

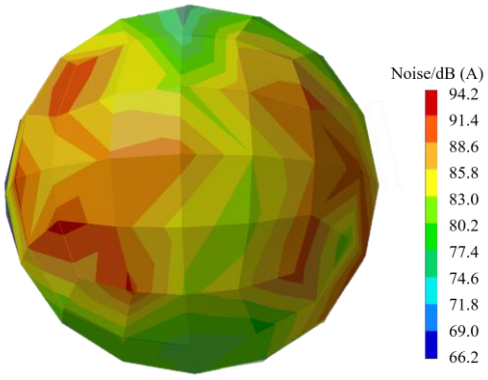

(b) Gangue coal seam

Figure 17. Noise response of cutting part drive system under different coal seams.

Figure 17 shows the noise radiation cloud diagrams at the peak frequency response for pure coal and gangue-intercalated working conditions. It is a front view from the goaf side toward the coal wall side along the traction direction of the shearer, consistent with the perspective shown in Figure 10(a). The noise level under extreme gangue-intercalated conditions is significantly higher than under pure coal conditions. For the pure coal condition, the noise response peak occurs above the positive slope of the rocker arm, where acoustic energy will be reflected by the coal wall surface in the fully mechanized mining face and transmitted to the receiver. For the gangue-intercalated condition, the acoustic radiation energy distribution is more dispersed, with high-amplitude noise occurring at the oblique rear and front of the traction direction, resulting in more extensive noise propagation in all directions.

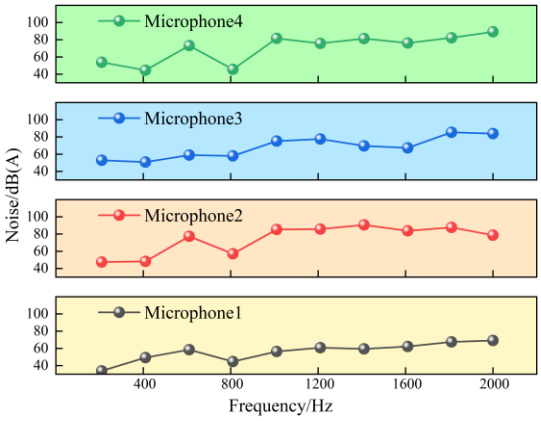

(a) Homogeneous coal seam

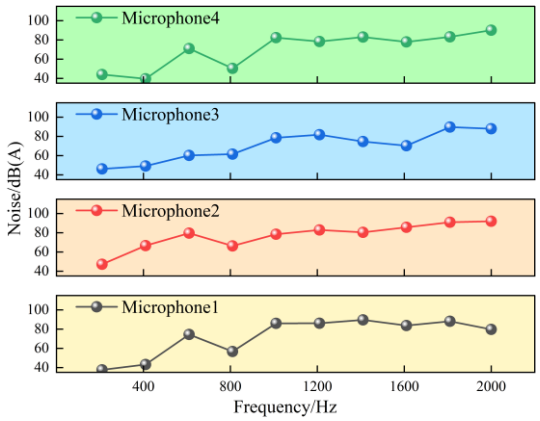

(b) Gangue coal seam

Figure 18. Noise frequency response curves at different microphones in the frequency response range.

Figure 18 shows the noise amplitude at different microphones in the 3 m sound field within the frequency response range. It can be seen from the figure that the noise radiation energy in the whole frequency response range is more

concentrated at the microphone 1 and 2 under the dirt band condition, that is, the left side of the rocker arm hinge hole and the upper position of the rocker arm. There are two microphones under the homogeneous coal seam, which are above the cutting part. The noise energy is low, and the noise amplitude at the other field points is very significant. As the excitation frequency continues to increase from 2000 Hz, the noise radiation values at microphones 2 and 4, that is, the upper position of the rocker arm and the traction position, continue to rise regardless of the dirt band condition or the pure coal condition.

3.4. The influence of gear macro parameters on system vibration and noise under the limit conditions of homogeneous coal seam and gangue coal seam

To reduce the system vibration and noise level under extreme working conditions, the influence of gear macro-geometry parameters on system NVH characteristics is quantitatively analyzed, and the optimal parameter combination is determined in this section. In order to further explore the vibration response of the cutting part system under different macro parameters, by changing the face width and bottom clearance coefficient of the gear, and performing vibration analysis in the Spectrum module, the selected structural parameters are ensured to improve the bearing reliability and reduce the vibration level. In order to explore the influence of face width on the vibration response characteristics of the system, and considering the limited space in the lubrication unit, the face width of the high-speed gear pair is increased to 71-75 mm respectively to analyze the maximum value of the frequency response range of 0-2000 Hz under multiple harmonic excitations of the high-speed gear pair. By changing the face width of the planetary gear train, the vibration response at the virtual measuring point under 135-140 mm is explored.

Figure 19 shows the effect of face width on the acceleration response at the virtual measurement points under extreme pure coal and gangue-intercalated conditions. Among the three points, the coal wall side end cover of motor gear Z3 (point 2) shows the largest response amplitude across all face width values. For virtual points 1 and 2 (high-speed stage end covers), the maximum acceleration of the high-speed gear first increases then decreases with increasing face width, reaching a minimum at 74 mm. For virtual point 3 (planetary gear housing), the vibration level is lowest at 136 mm face width under pure coal conditions, while under gangue-intercalated conditions, the minimum peak acceleration occurs at 140 mm face width. Therefore, setting the high-speed gear face width to 74 mm and the planetary gear train face width to 140 mm is optimal for reducing system vibration within the space constraints of the lubrication oil chamber.

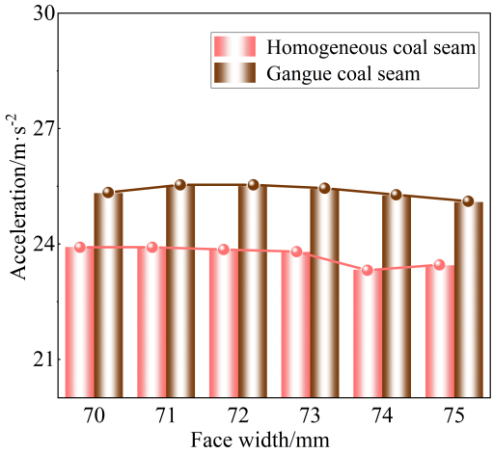

(a) Virtual point 1

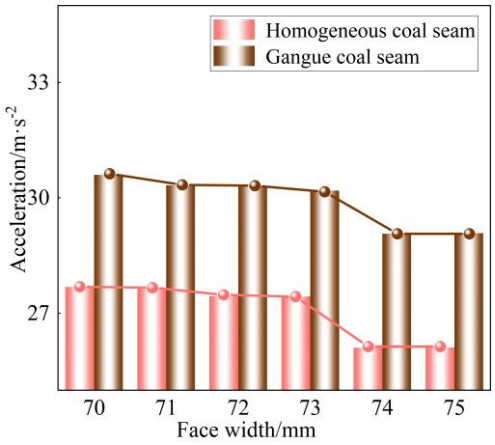

(b) Virtual point 2

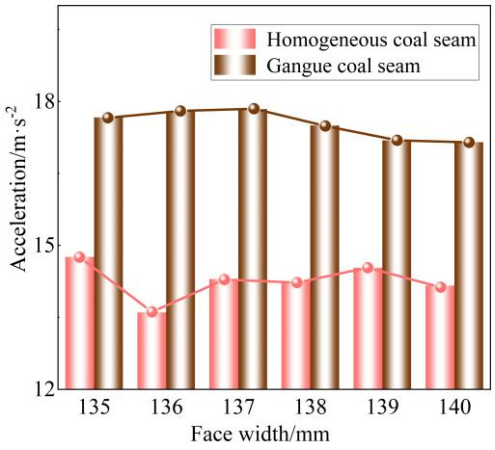

(c) Virtual point 3

Figure 19. Acceleration response amplitude under different face widths.

To investigate the effects of bottom clearance on system vibration response, simulations were performed with bottom clearance coefficients of 0.25, 0.3, 0.35, and 0.4, analyzing the frequency response in the 0–2000 Hz range under high-speed gear harmonic excitation.

Figure 20 shows the effect of the bottom clearance coefficient on the acceleration response at the virtual measurement points. At virtual point 1 (motor gear Z1 end cover) and point 3 (planetary reducer), the peak acceleration increases slightly with increasing clearance, with a slow increase at point 1 and a more noticeable increase at point 3. For virtual point 2 (motor gear Z3 end cover), which has the highest vibration level, the peak acceleration decreases at a clearance coefficient of 0.35, with the most significant reduction under pure coal conditions. Comprehensive analysis of all three measurement points shows that a bottom clearance coefficient of 0.4 is optimal for minimizing overall system vibration.

The change of gear macro parameters, such as face width and bottom clearance, can not only change the loading characteristics of tooth surface, but also affect the noise of cutting part transmission system. In order to explore the influence of the macroscopic parameters of the system on the sound field radiation of the system, the shell with vibration vector under different planetary gear train face width and bottom clearance coefficient is imported into LMS virtual.lab for boundary element noise analysis. Based on the existing literature on the noise characteristics of the gearbox, due to the high density and compact structure of the planetary gear train, the vibration energy transmitted to the shell is more concentrated, and the high-speed stage has less effect on the sound field of the 3m radius. Therefore, only the influence of the change of the macroscopic parameters of the planetary gear on the radiation noise of the system is discussed. In order to explore the influence of face width on the noise radiation of the system, the sound field characteristics of the system noise are analyzed when the face width of the planetary gear train is adjusted to 135-140 mm respectively.

Figure 21(a) shows the maximum noise amplitude at different virtual microphones as a function of planetary gear train face width. At virtual microphone 2, the noise difference between gangue-intercalated and pure coal conditions remains large across all face width values. Across all microphones, the noise response amplitude peaks at a planetary gear train face width of 136 mm, which should be avoided in the structural optimization of the planetary gear train. The noise amplitude is lowest at face widths of 135 mm and 140 mm, with negligible difference between the two.

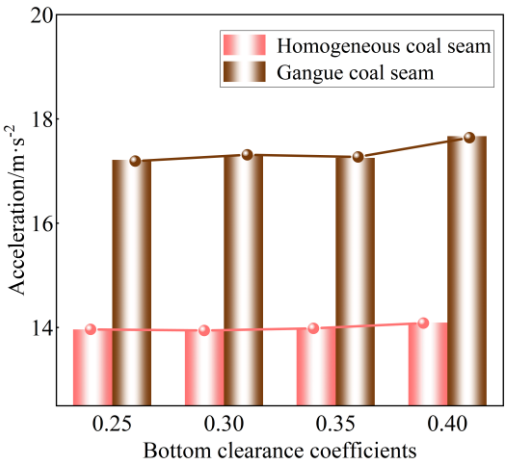

(a) Virtual point 1

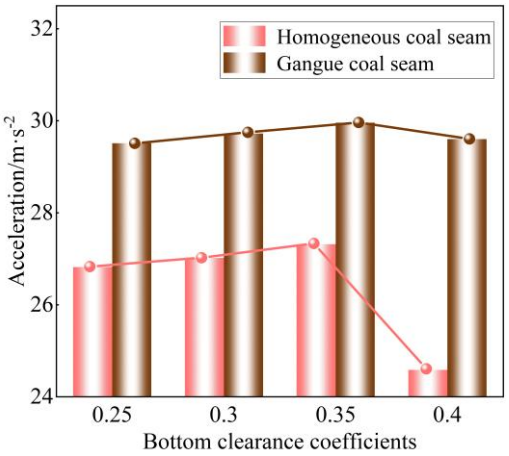

(b) Virtual point 2

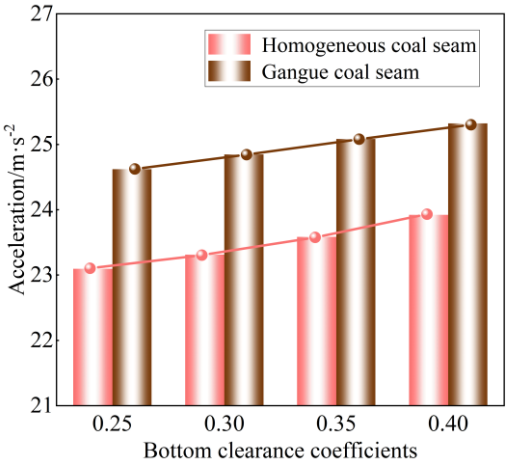

(c) Virtual point 3

Figure 20. Acceleration response amplitude under different bottom clearances.

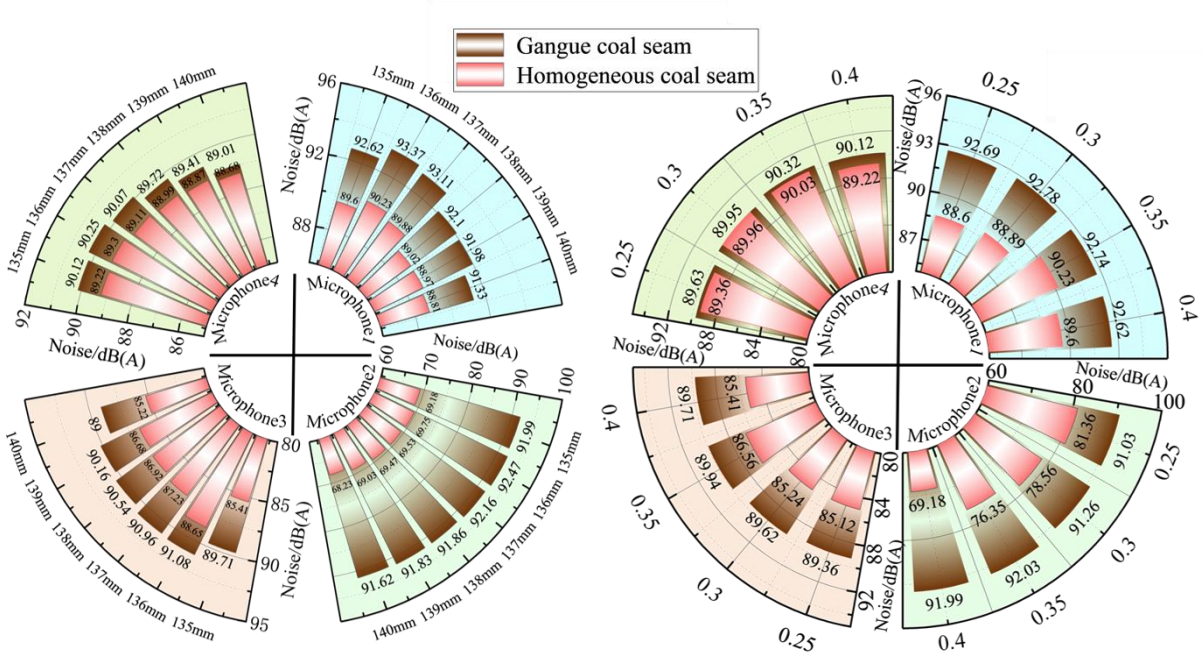

(a) Different face widths (b) Different bottom clearance coefficients

Figure 21. Noise response values at different microphones.

The bottom clearance size is controlled by the bottom clearance coefficient, which not only affects the accumulated heat at the tooth root to be taken away by the lubricating oil, but also has a certain influence on the vibration and noise characteristics. The noise radiation characteristics of the 3-meter free sound field of the gear transmission system of the cutting part are investigated under the bottom clearance coefficient of 0.25, 0.3, 0.35 and 0.4. Figure 21(b) shows the maximum noise amplitude at different virtual microphones as a function of the planetary gear train bottom clearance coefficient. The bottom clearance coefficient has the least effect on the noise response at virtual microphone 4, with noise levels decreasing with increasing bottom clearance for both working conditions. For the other three microphones, the noise level under gangue-intercalated conditions increases slowly with increasing bottom clearance, while under pure coal conditions, the maximum noise response is similar for bottom clearance coefficients of 0.25 and 0.4.

From the perspective of reducing omnidirectional noise, there is minimal difference between bottom clearance coefficients of 0.25 and 0.4 for the planetary gear train design. However, a larger bottom clearance can store more lubricating oil and improve heat dissipation, which helps avoid tooth root bending fatigue. Therefore, a bottom clearance coefficient of 0.4 is prioritized for comprehensive optimization.

4. Conclusion

(1) A coupling verification method combining test bench testing and Romax simulation is established for the dynamic characteristics of the shearer cutting unit transmission system. In the boundary condition setting, rigid fixed constraints are applied at the hinge of the rocker arm to simplify the simulation model. This study provides a general verification idea for the dynamic simulation of similar mine gear transmission systems, and addresses the problem of low reliability of simulation models in existing research due to the lack of physical test verification.

(2) Modal analysis results show that the first 40 natural frequencies of the system are distinctly separated from the gear meshing frequencies, shaft rotational frequencies and their harmonic components, indicating no resonance risk exists in the system. The mode shapes prone to resonance are mainly concentrated on high-speed components and the planetary reducer. Under extreme gangue intercalation conditions, the dynamic bearing contact force, housing vibration acceleration and

noise radiation level of the system are remarkably higher than those under pure coal working conditions. The bearings of the five-axis assembly at the high-speed stage and the coal-wall side bearings of the planet carrier withstand the maximum dynamic contact force. The gravity direction dominates the main vibration direction of the gearbox housing. The noise radiation energy is concentrated under pure coal conditions, while presenting an omnidirectional distribution under gangue intercalation conditions.

(3) The quantitative influence laws of gear face width and bottom clearance coefficient on system vibration and noise are revealed, and a collaborative optimization scheme for gear macro geometric parameters is proposed. The optimal parameter combination is determined as follows: motor gear face width of 74 mm, planetary gear train face width of 140 mm, and a bottom clearance coefficient of 0.4. The scheme realizes the collaborative optimization of system load-bearing capacity, vibration reduction and noise reduction, which can provide a scientific reference for the structural design and performance improvement of the shearer cutting unit transmission system.

Although the dynamic and noise characteristics of the shearer cutting unit transmission system have been clarified by combining experimental tests and numerical simulations, several limitations still remain in this study. The rigid constraint adopted at the rocker arm hinge may slightly overestimate the natural frequency and vibration amplitude, resulting in a noise simulation deviation within 3～5 dB(A). Meanwhile, the numerical calculation fails to consider the noise attenuation effect of underground humidity, dust and temperature, as well as the sound reflection and scattering caused by coal walls and hydraulic supports, making the simulated noise value 2～4 dB(A) higher than the actual underground measured data. In addition, the research is only carried out based on laboratory bench tests and numerical simulations, without underground industrial test verification. In subsequent research, model parameters will be revised and calibrated combined with field measured data, to further improve the model accuracy and engineering applicability.

References

1. Wang L, Zhang D, Wang D, Feng C. A Review of Selected Solutions on the Evaluation of Coal-Rock Cutting Performances of Shearer Picks under Complex Geological Conditions. *Applied Sciences* 2022; 12(23): 12371. https://doi.org/10.3390/app122312371.
2. Zhao LJ, Tian Z. Application of Co-Simulation in Noise and Vibration Analysis of Shearer. *Advanced Materials Research* 2012; 619: 172-5. https://doi.org/10.4028/www.scientific.net/amr.619.172.
3. Du W, Li W, Jiang S, Sheng L, Wang Y. Nonlinear torsional vibration analysis of shearer semi-direct drive cutting transmission system subjected to multi-frequency load excitation. *Nonlinear Dynamics* 2023; 111: 4071-4086. https://doi.org/10.1007/s11071-022-08041-x.
4. Lv Y, Zhao J, Miao B, Chang H, Ren X. Optimal Cooperative Controls for Multi-motor Driving System in Long-wall Shearer. *International Journal of Control*, Automation and Systems 2024; 22: 2686-2698. https://doi.org/10.1007/s12555-023-0174-4.
5. Sheng L, Li W, Ye G, Jiang S, Li Y. Stability and combined vibration of gear transmission system in shearer cutting section under multi-parameter excitation. *International Journal of Dynamics and Control* 2021; 9: 392-402. https://doi.org/10.1007/s40435-020-00687-y.
6. Jin L, Shao J, Wang X, Wang Y, Fu B. Vibroacoustic characteristics analysis of a planetary gear reducer considering the exterior housing structure. *Mechanical Sciences* 2021; 12: 539-557. https://doi.org/10.5194/ms-12-539-2021.
7. Hartlieb S, Ringkowski M, Haist T, Sawodny O, Osten W. Multi-positional image-based vibration measurement by holographic image replication. *Light: Advanced Manufacturing* 2021; 2: 32. https://doi.org/10.37188/lam.2021.032.
8. Souza MR, Haris A, Rodrigues L, Offner G, Schöpflin M, Diwoky R, Mohammadpour M, Theodossiadis S. The use of an artificial neural network for assessing tone perception in electric powertrain noise, vibration and harshness. *Meccanica* 2024; 59: 433-459. https://doi.org/10.1007/s11012-024-01753-x.
9. Zhu Y, Zhang S, Tang S, Chang Z, Lin R, Zhang L. Dynamic Characteristics Analysis of the DI-SO Cylindrical Spur Gear System Based on Meshing Conditions. *Journal of Marine Science and Engineering* 2024; 12(9): 1589. https://doi.org/10.3390/jmse12091589.
10. Huang D, Li Y, Zheng X, Li G. Study on Dynamic Behaviors of Hypoid Gears Under Variable Tidal Current Energy Harvesting Conditions. *Machines* 2025; 13(3): 178. https://doi.org/10.3390/machines13030178.

11. Guan Y, Li M, Lim C T, Shepard W. Comparative analysis of actuator concepts for active gear pair vibration control. *Journal of Sound and Vibration* 2004; 269(1-2): 273-294. https://doi.org/10.1016/S0022-460X(03)00072-5.
12. Kim S J, Lee S K. Experimental identification on a gear whine noise in the axle system of a passenger van. *International Journal of Automotive Technology* 2007; 8(1): 75-82.
13. Zhou J, Sun W, Cao L. Vibration and noise characteristics of a gear reducer under different operation conditions. *Journal of Low Frequency Noise, Vibration and Active Control* 2019; 38(2): 574-591. https://doi.org/10.1177/1461348419825603.
14. Schweigert D, Morhard B, Oberneder F, Pointner-Gabriel L, Otto M. Numerical and experimental investigations on the vibration behavior of a high-speed planetary gearbox. *Forsch Ingenieurwes* 2024; 88: 7. https://doi.org/10.1007/s10010-024-00727-5.
15. Mughal H, Sivayogan G, Dolatabadi N, Rahmani R. An efficient analytical approach to assess root cause of nonlinear electric vehicle gear whine. *Nonlinear Dynamics* 2022; 110: 3167-3186. https://doi.org/10.1007/s11071-022-07800-0.
16. Pietrusiak D, Wróbel J, Czechowski M, Fiebig W. Dynamic NVH Numerical Analysis of Power Steering in the Presence of Lubricant in the System. *Materials* 2022; 15(7): 2406. https://doi.org/10.3390/ma15072406.
17. Hong C, Liu M, Su N, Zou S, Xiao J, Xu C, Zhu F. Study on the Influence of Gear Spoke Hole Numbers on Meshing Noise. *Applied Sciences* 2023; 13(1): 511. https://doi.org/10.3390/app13010511.
18. Huang B, Tan B, Wang J, Liu K, Zhang Y. NVH Analysis and Optimization of Construction Hoist Drive System. *Energies* 2023; 16(17): 6199. https://doi.org/10.3390/en16176199.
19. Tanaka E, Houjoh H, Mutoh D, Motoshiromizu H, Ohno K, Tanaka N. Vibration and sound-radiation analysis for designing a low-noise gearbox with a multi-stage helical gear system. *JSME International Journal Series C Mechanical Systems, Machine Elements and Manufacturing* 2003; 46(3): 1178-1185. https://doi.org/10.1299/jsmec.46.1178.
20. Liu C, Qin D, Liao Y. Electromechanical dynamic analysis for the drum driving system of the long-wall shearer. *Advances in Mechanical Engineering* 2015; 7(10). https://doi.org/10.1177/1687814015612031.
21. Sheng L, Li W, Jiang S, Sheng J, Li A. Nonlinear torsional vibration analysis of motor rotor system in shearer semi-direct drive cutting unit under electromagnetic and load excitation. *Nonlinear Dynamics* 2019; 96: 1677-1691. https://doi.org/10.1007/s11071-019-04878-x.
22. Feng K, Ji JC, Ni Q, Beer M. A review of vibration-based gear wear monitoring and prediction techniques. *Mechanical Systems and Signal Processing* 2023; 182: 109605. https://doi.org/10.1016/j.ymssp.2022.109605.
23. Schanz M .Realizations of the generalized adaptive cross approximation in an acoustic time domain boundary element method. *PAMM* 2023; 23(2). https://doi.org/10.1002/pamm.202300024.
24. Lao J, Chen Z, Wang X, Zhang M, Guo J. Optimization of Coal Mining Machine Drum Structure and Microscopic Analysis of Coal Particle Flow. *Energy Science & Engineering* 2025; 13: 1442-1456. https://doi.org/10.1002/ese3.70028.
25. Zhao L ,Liu H ,Zhou W .A Study on the Dynamic Transmission Law of Spiral Drum Cutting Coal Rock Based on ANSYS/LS-DYNA Simulation. *Complexity* 2019; 20191482051: 1-1482051:14. https://doi.org/10.1155/2019/1482051.
26. Sheng L, Li W, Ye G, Jiang S. Nonlinear dynamics characteristics of motor rotor system in shearer cutting section considering electromechanically coupled effect. *Journal of Mechanical Science and Technology* 2021; 35: 3281-3291. https://doi.org/10.1007/s12206-021-0702-1.
27. Yang W, Tang X. Modelling and modal analysis of a hoist equipped with two-stage planetary gear transmission system. *Proceedings of the Institution of Mechanical Engineers, Part K: Journal of Multi-body Dynamics* 2017; 231(4): 739-749. https://doi.org/10.1177/1464419316684067.
28. Liao J, Yu H, Yan J, Hsu SH. Simulation and Modal Analysis of Marine Diesel Engine Based on Finite Element Model and Vibration Sensor Data. *Sensors and Materials* 2021; 33(5(2)): 1645-1656. https://doi.org/10.18494/SAM.2021.3180.
29. Lei Y, Hou L, Fu Y, Hu J, Chen W. Research on vibration and noise reduction of electric bus gearbox based on multi-objective optimization. *Applied Acoustics* 2020; 158: 107037. https://doi.org/10.1016/j.apacoust.2019.107037.
30. Pizzolante F, Battarra M, Mucchi E. The role of gear layout and meshing phase for whine noise reduction in ordinary gear trains. *Mechanism and Machine Theory* 2023; 181: 105209. https://doi.org/10.1016/j.mechmachtheory.2022.105209.